Iowa State University
Digital Repository

Retrospective Theses and Dissertations

Iowa State University Capstones, Theses and Dissertations

2007

Piezoelectric coupling constant in epitaxial Mg-doped GaN and design of pentacene acoustic charge transfer devices

Xiaofeng Xu
Iowa State University

Follow this and additional works at: https://lib.dr.iastate.edu/rtd

Part of the Electrical and Electronics Commons

Recommended Citation
Xu, Xiaofeng, "Piezoelectric coupling constant in epitaxial Mg-doped GaN and design of pentacene acoustic charge transfer devices" (2007). *Retrospective Theses and Dissertations*. 15021.
https://lib.dr.iastate.edu/rtd/15021

This Thesis is brought to you for free and open access by the Iowa State University Capstones, Theses and Dissertations at Iowa State University Digital Repository. It has been accepted for inclusion in Retrospective Theses and Dissertations by an authorized administrator of Iowa State University Digital Repository. For more information, please contact digirep@iastate.edu.

المنارة للاستشارات

www.manaraa.com

Piezoelectric coupling constant in epitaxial Mg-doped GaN and design of pentacene acoustic charge transfer devices

by

Xiaofeng Xu

A thesis submitted to the graduate faculty

in partial fulfillment of the requirements for the degree of

MASTER OF SCIENCE

Major: Electrical Engineering

Program of Study Committee:
Clive Woods, Major Professor
Jiming Song
Kai-Ming Ho

Iowa State University

Ames, Iowa

2007

Copyright © Xiaofeng Xu, 2007. All rights reserved.

المنارة للاستشارات

www.manaraa.com

UMI Number: 1443737

UMI®

UMI Microform 1443737

Copyright 2007 by ProQuest Information and Learning Company.
All rights reserved. This microform edition is protected against
unauthorized copying under Title 17, United States Code.

ProQuest Information and Learning Company
300 North Zeeb Road
P.O. Box 1346
Ann Arbor, MI 48106-1346

المنارة للاستشارات

www.manaraa.com

TABLE OF CONTENTS

LIST OF FIGURES v

ABSTRACT vii

CHAPTER 1. INTRODUCTION 1

1.1 Surface acoustic wave devices 1

1.2 Acoustic charge transfer devices 2

1.3 Thesis organization 3

CHAPTER 2. BASICS OF SURFACE ACOUSTIC WAVES AND PIEZOELECTRICITY 5

2.1 Surface acoustic wave in a non-piezoelectric elastic solid medium 5

2.1.1 Wave equations 5

2.1.2 Surface acoustic wave 6

2.2 Surface acoustic wave in a piezoelectric elastic solid medium 8

2.3 Basics of interdigital transducers 9

2.3.1 The structure of a typical interdigital transducer 9

2.3.2 The principle of interdigital transducer operation 9

2.3.3 Electrode reflections of an IDT 11

CHAPTER 3. THE FUNDAMENTALS OF ACT DEVICES 13

3.1 Basic ACT operations 13

3.2 SAW power requirements 14

3.3 Structures of charge transport channels in ACT devices 16

www.manaraa.com

CHAPTER 4. PIEZOELECTRIC COUPLING CONSTANT IN EPITAXIAL Mg-DOPED GaN 19

4.1 Introduction 19

4.2 Experiment 20

4.2.1 Design of SAW filters 20

4.2.2 Fabrication of SAW filters 21

4.2.3 Measurement 22

4.3 Results and Discussion 23

4.4 Conclusions 28

CHAPTER 5. DESIGN OF PENTACENE ACOUSTIC CHARGE TRANSFER DEVICES 30

5.1 Introduction 30

5.2 Design of acoustic charge transfer devices using pentacene 31

5.3 Design of a parabolic SAW beam compressor 35

5.4 Design of masks 39

5.5 Distillation of pentacene 40

5.5.1 The reasons of pentacene distillation 40

5.5.2 The design of a temperature gradient furnace 40

5.5.3 Operation of the furnace 43

5.6 Fabrication of pentacene ACT devices 44

5.7 Conclusions 47

CHAPTER 6. CONCLUSIONS AND FUTURE WORK 48

6.1 Conclusions 48

المنارة للاستشارات

www.manaraa.com

6.2 Future work 49

APPENDIX A. EQUATIONS OF MOTION IN A HOMOGENEOUS SOLID MEDIUM 50

APPENDIX B. WAVE EQUATIONS IN A PIEZOELECTRIC ELASTIC MEDIUM 53

REFERENCES 55

ACKNOWLEDGEMENTS 60

المنارة للاستشارات

www.manaraa.com

LIST OF FIGURES

Figure 2.1 Axes for SAW analysis 6

Figure 2.2 Schematic structure of a uniform IDT with single electrodes 10

Figure 2.3 Electric field distributions of an IDT 10

Figure 2.4 Reflections from the electrodes of a single finger IDT 11

Figure 2.5 Structure of a uniform periodic IDT with double electrodes 12

Figure 2.6 Reflections from the electrodes of a double finger IDT 12

Figure 3.1 Schematic cross section of a basic ACT delay line 13

Figure 3.2 Cross section of an ACT device with a depletion channel 16

Figure 3.3 Cross section of an ACT with a thin film channel. 17

Figure 3.4 Cross section of an ACT with a quantum well channel 17

Figure 3.5 Cross section of an ACT device with a single heterojunction channel 18

Figure 4.1 Schematic diagram of a SAW filter 20

Figure 4.2 Photograph of the device 22

Figure 4.3 Schematic diagram of the experimental arrangement for time response measurement 23

Figure 4.4 A typical Smith chart of reflection coefficient for an interdigital transducer 24

Figure 4.5 Smith chart of reflection coefficient for all devices 25

Figure 4.6 Simple equivalent circuit model used to estimate the IDT transduction loss 26

Figure 4.7 Time response of SAW filters to an RF pulse 28

Figure 5.1 A comparison of the advantages and disadvantages of different beam compression methods 32

المنارة للاستشارات

www.manaraa.com

Figure 5.2 Plan view of pentacene ACT configuration 34

Figure 5.3 Geometry of beam compressor 35

Figure 5.4 Schematic diagram of a temperature gradient furnace 41

Figure 5.5 The temperature profile of the furnace 44

Figure 5.6 Photos of the pentacene layer 45

Figure 5.7 Photo of a good pentacene charge transfer channel 46

Figure A.1 Forces exerted on an infinitesimal volume element 50

المنارة للاستشارات

www.manaraa.com

ABSTRACT

Surface acoustic wave (SAW) filters were fabricated on an Mg-doped GaN epilayer using liftoff photolithography. The measurement of the time response showed that these devices had very weak output signals. The center frequencies were 136.09MHz, 114.48MHz and 98.64MHz for devices with wavelengths of 40µm, 48µm and 56µm, respectively. No change of the reflection coefficient was detectable using the available network analyzer for all devices around the center frequencies. The insertion loss for all devices was higher than 80dB. The upper bound of the electromechanical coupling coefficient (K^2) of the Mg-doped GaN epilayer was calculated to be 1×10^{-4}%. This is much less than other III-V materials, and so this material does not appear to be promising for SAW applications.

A design of an acoustic charge transfer (ACT) device which has been previously proposed with pentacene as the charge transfer channel is discussed. Because the charge mobility of pentacene is very small, the minimum requirement of the SAW power per unit acoustic aperture was calculated to be very high. In order to reduce the required electrical drive power, a parabolic SAW beam compressor was used and the detailed design of the parabolic compressor is given. It is known that commercially available pentacene contains nonnegligible amounts of impurities so that its charge mobility will be low. Therefore, a temperature gradient furnace was set up to distill pentacene to improve the carrier mobility. The device is expected to be fabricated using standard liftoff photolithographic techniques. However, some problems were met when the pentacene charge transfer channel was fabricated. Solutions, such as heating the substrate during the deposition and growing some other material between pentacene and the substrate as an adhesive, are under investigation.

www.manaraa.com

CHAPTER 1. INTRODUCTION

1.1 Surface acoustic wave devices

Surface acoustic waves (SAWs) have been studied for over a hundred years. SAWs were first reported as elastic waves propagating along a surface of a solid by Lord Rayleigh in 1885 [1]. However, for a long time, SAW had not been applied to electronic devices because of the lack of efficient generation and detection. In 1965, White and Voltmer [2] reported that an interdigital transducer (IDT) could efficiently excite a SAW in a piezoelectric solid if a sinusoidal voltage was applied to it. This invention made SAW attract many interests. Since SAWs can transfer electrical signals through IDTs, their great advantages in signal processing were soon realized. Many SAW devices then started to be explored. Some of them were soon successful and found their first applications in military systems. Since then, with the development of SAW devices, they have found more and more applications in different areas. Today, SAW devices have been widely used in consumer, commercial, and military systems. For consumer applications, SAW devices, such as filters, resonators and delay lines, can be commonly seen in TV sets, VCRs, Satellite TV receivers, cell phones, cordless phones, pagers, keyless entry systems, home and car security systems, and medical alert devices [3-4]. For commercial applications, they provide state-of-the-art performance to many systems, including CATV/MATV (cable television and master antenna television) headends, local area networks, satellite data receivers, digital microwave systems, fiber optical repeaters, TV test equipments, RF synthesizers, and spectrum analyzers [4]. For military applications, SAW devices play key roles in radar, electronic warfare, electronic counter measure, electronic counter counter measure, and distance measure systems [4].

المنارة للاستشارات
www.manaraa.com

The huge success of SAW devices is due to their excellent performance features when compared to competing technologies. These include [5]:

1. SAW devices can provide complex signal processing functions within a single package.
2. SAW devices can be mass produced using semiconductor fabrication techniques so that they are cost competitive in mass-volume applications.
3. SAW devices can have outstanding reproducibility in performance, from device to device.
4. SAW devices can be implemented in small, rugged, light and power efficient modules.
5. SAW devices can be employed in many digital communication systems.
6. SAW filters can be made to operate very efficiently at high-harmonic modes [6].

1.2 Acoustic charge transfer devices

In 1982, Hoskins *et al.* [7] demonstrated the first successful acoustic charge transfer (ACT) device. After that, the primary development of ACT technology was mainly focused on the device architecture used to achieve electrical transfer channel isolation [8]. In 1987, Hoskins and Hunsinger [8] reviewed the development of ACT devices at that time. They discussed four ACT device functional capabilities and demonstrated the signal processing performance of an ACT delay line, transversal filter, and a spread spectrum correlator. Following that, a wide range of ACT signal processors was developed. For example, Hunsinger [9] described a signal microprocessor enabled by ACT technology; Bales *et al.* [10] reported a GaAs ACT/IC programmable wide-band analog siganal processor; and Miller

المنارة للاستشارات
www.manaraa.com

et al. [11] reported a programmable transversal filter which could execute 2×10^{10} multiply and sum operations per second. In 1993, Vigil *et al.* [12] reported seven areas to which the application of ACT technology was at some stage of development. Unlike a SAW device which only processes signals with a selected frequency, an ACT device just uses the SAW as a "clock" to sample signals. Therefore, an ACT device can be made programmable and under control of a digital processor. This is the most attractive feature of the ACT technology and it makes ACT devices well suit for certain intensive, repetitive, pipelined operations like convolution and correlation, which are hard to do efficiently on a digital computer. The applications of ACT devices are wide. They include pulse compression, multichannel matching, waveform generation, clutter cancellation, Doppler processing, and beamforming in radar systems; signal sorting, signal characterization, and false signal generation in electronic warfare; and spread spectrum correlators, band shaping, equalization, and coded waveform generation [13].

1.3 Thesis organization

This thesis is divided into five remaining chapters. Chapter 2 briefly reviews the theory of SAW. Wave equations of SAWs in different materials are given. The operation of an IDT is also briefly described in Chapter 2. Chapter 3 introduces basics of an ACT device. In this chapter the basic operation of an ACT device is described. In order to make an ACT device work, the minimum requirement of SAW power must be achieved. The calculation of the minimum requirement is discussed. In this chapter, different structures of the ACT devices are also briefly described. Chapter 4 discusses the measurement of the piezoelectric coupling constant in epitaxial Mg-doped GaN. Chapter 5 discusses the design of a pentacene

المنارة للاستشارات
www.manaraa.com

ACT device and describes the problems met during the fabrication of the devices. Chapter 6 will provide a project summary and a discussion regarding future work.

المنارة للاستشارات
www.manaraa.com

CHAPTER 2. BASICS OF SURFACE ACOUSTIC WAVES AND PIEZOELECTRICITY

2.1 Surface acoustic wave in a non-piezoelectric elastic solid medium

2.1.1 Wave equations

In a homogenous solid medium, the equations of motion of a particle in Cartesian coordinate system is [14]

$$\rho \frac{\partial^2 u_i}{\partial t^2} = \sum_{j=1}^{3} \frac{\partial T_{ij}}{\partial x_j} \qquad (i=1, 2, 3). \qquad (2.1)$$

where ρ is the density of the medium, u_i is the x_i component of the displacement of the infinitesimal volume element and T_{ij} is the x_i component of the stress acting on a surface normal to x_j axis. The detailed derivation is shown in Appendix A. Using the Einstein summation convention which implies that when an index occurs more than once in the same expression, the expression is implicitly summed over all possible values for that index, (2.1) can be reduced to

$$\rho \frac{\partial^2 u_i}{\partial t^2} = \frac{\partial T_{ij}}{\partial x_j} \qquad (i, j=1, 2, 3). \qquad (2.2)$$

If the solid medium is non-piezoelectric, according to Hooke's law, the stresses can be written as

$$T_{ij} = c_{ijkl} S_{kl} \qquad (i, j, k, l=1, 2, 3), \qquad (2.3)$$

where c_{ijkl} are the components of the elastic stiffness tensor, and S_{kl} are the components of the strain tensor and defined as

المنارة للاستشارات
www.manaraa.com

$$S_{kl} = \frac{1}{2}\left(\frac{\partial u_k}{\partial x_l} + \frac{\partial u_l}{\partial x_k}\right). \tag{2.4}$$

Because $c_{ijkl}=c_{ijlk}$ [15], substituting (2.4) into (2.3) yields

$$T_{ij} = c_{ijkl}\frac{\partial u_k}{\partial x_l}. \tag{2.5}$$

Substitution of (2.5) into (2.2) leads to

$$\rho\frac{\partial^2 u_i}{\partial t^2} = c_{ijkl}\frac{\partial^2 u_k}{\partial x_j \partial x_l} \qquad (i, j, k, l=1, 2, 3). \tag{2.6}$$

These are the wave equations in a non-piezoelectric elastic solid medium. Solving these equations will give the characteristics of all elastic waves in the medium.

2.1.2 Surface acoustic waves

Consider an elastic solid medium with infinite extent in the x_1 and x_3 directions but with a boundary at x_3=0, so that the medium occupies the space x_3<0 and the space x_3>0 is a free space, as shown in Figure 2.1. Therefore, the solutions to the wave equations (2.6) must satisfy the following boundary condition:

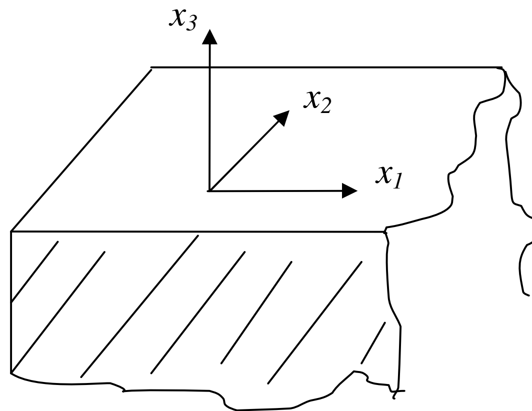

Figure 2.1 Axes for SAW analysis.

المنارة للاستشارات
www.manaraa.com

$$T_{31} = T_{32} = T_{33} = 0 \qquad \text{at} \qquad x_3=0. \tag{2.7}$$

If the elastic solid medium is isotropic and a SAW propagates along the x_1 axis, the SAW solution to (2.6) which satisfies the boundary condition (2.7) is given by [16]

$$\begin{aligned} u_1 &= C[\exp(kb_1x_3) - A\exp(kb_2x_3)]\exp[ik(x_1 - vt)] \\ u_2 &= 0 \\ u_3 &= -ib_1C\left[\exp(kb_1x_3) - \frac{1}{A}\exp(kb_2x_3)\right]\exp[ik(x_1 - vt)], \end{aligned} \tag{2.8}$$

where

$$\begin{aligned} b_1 &= \left(1 - v^2 / v_l^2\right)^{1/2} \\ b_2 &= \left(1 - v^2 / v_t^2\right)^{1/2} \\ A &= (b_1 b_2)^{1/2} \end{aligned}$$

and v_t, v_l are the velocities of the bulk shear wave and the bulk longitudinal wave, respectively. The SAW described by (2.8) is also called a Rayleigh wave.

It is obvious from (2.8) that the particle displacement vector of a Rayleigh wave only has two components: one is along the x_1 axis and the other is along the x_3 axis, and there is a $\pi/2$ phase shift between u_1 and u_3. Therefore, the particle trace of a Rayleigh wave is an ellipse. Since the amplitudes of u_1 and u_3 exponentially decrease with x_3, the shape of the ellipse changes with x_3 and the disturbance becomes negligible for depths more than a few wavelengths from the surface.

If the elastic solid medium is anisotropic, solving the wave equations (2.6) becomes very intricate and usually can only be done numerically. The SAW in an anisotropic medium will have some different properties from that in an isotropic medium [15].

- The surface wave velocity depends on the direction of propagation in the free surface plane except if this plane is orthogonal to a six-fold axis.

المنارة للاستشارات
www.manaraa.com

- If the sagittal plane (x_1x_3 plane) is not a symmetry plane the elastic properties, the displacement vector has three components and it runs along an ellipse.
- Generally, the energy flux is not parallel to the propagation direction. Only at the surface of selected planes and for specific direction, they can be in the same direction.

2.2 Surface acoustic wave in a piezoelectric elastic solid medium

As shown in detail in Appendix B, the wave equations in a piezoelectric material are [14]:

$$\rho \frac{\partial^2 u_i}{\partial t^2} = c_{ijkl}^E \frac{\partial^2 u_k}{\partial x_l \partial x_k} + e_{kij} \frac{\partial^2 \Phi}{\partial x_k \partial x_j}. \qquad (2.9)$$

$$e_{jkl} \frac{\partial^2 u_k}{\partial x_l \partial x_j} - \varepsilon_{jk} \frac{\partial^2 \Phi}{\partial x_k \partial x_j} = 0. \qquad (2.10)$$

where c_{ijkl}^E is the elastic constant when the electric field is a constant, e_{kij} is the piezoelectric constant, Φ is electric potential, and ε_{jk} is the components of the dielectric constant of the piezoelectric material. A solution to the equation set of (2.9) and (2.10) also needs to satisfy the mechanical and electric boundary conditions:

$$\begin{aligned} & c_{i3kl} \frac{\partial u_k}{\partial x_l} + e_{k3j} \frac{\partial \Phi}{\partial x_k} = 0 \\ & e_{3kl} \frac{\partial u_k}{\partial x_l} - \varepsilon_{3k} \frac{\partial \Phi}{\partial x_k} = -\varepsilon_0 \frac{\partial \Phi}{\partial x_3} \\ & \nabla^2 \Phi = 0 \qquad\qquad (x_3 > 0). \end{aligned}$$

The SAW solution can only be found by numerically solving the equation set (2.9) and (2.10) with the above boundary conditions. Since the effect of the piezoelectricity is to

المنارة للاستشارات
www.manaraa.com

increase the effective elastic constants [16], an electromechanical coupling constant K^2 can be used to describe this effect. The electromechanical coupling constant K^2 is defined as [16]

$$K_{ijkl}^2 = \frac{e_{mij} e_{nkl} n_m n_n}{c_{ijkl} \varepsilon_{jk} n_j n_k}, \qquad (i, j, k, l, m, n=1, 2, 3)$$

where n_i is the direction cosine of the wave propagation direction with respect to the Cartesian axis x_i. Therefore, the SAW in a piezoelectric medium has similar properties as that in an anisotropic non-piezoelectric medium. Besides, along with the propagation of the SAW, there exists a traveling electric field moving at the same speed as the SAW. That traveling electric field is the very basis of an acoustic charge transfer device.

2.3 Basics of interdigital transducers

2.3.1 The structure of a typical interdigital transducer

Interdigital transducers (IDTs) are used to generate and detect SAWs on the surface of a piezoelectric substrate. They are the building blocks of surface wave filters. Generally, IDTs comprise two sets of metallic electrodes which are interleaved with each other and periodically arranged in a plane. Figure 2.2 schematically shows the structure of an uniform periodic IDT with single electrodes. In this structure, the width of each electrode and the spacing between the adjacent two electrodes are $\lambda/4$, where λ is the SAW wavelength.

2.3.2 The principles of interdigital transducer operation

When voltage is applied to an IDT, an electric field distribution in the substrate will be established between the electrodes, as shown in Figure 2.3 [14]. These electric fields have a spatial period same as that of the IDT electrodes. If the IDT is made on the surface of a piezoelectric substrate, then because of piezoelectric coupling, these electric fields can

المنارة للاستشارات
www.manaraa.com

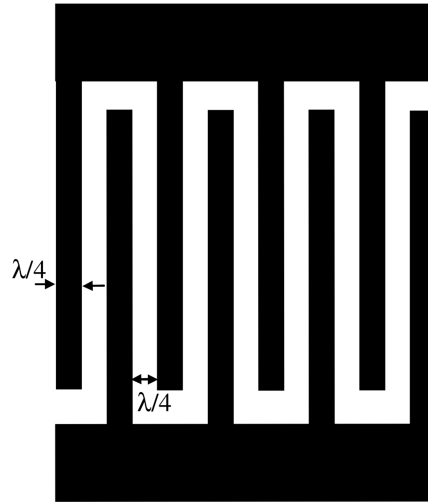

Figure 2.2 Schematic structure of a uniform IDT with single electrodes.

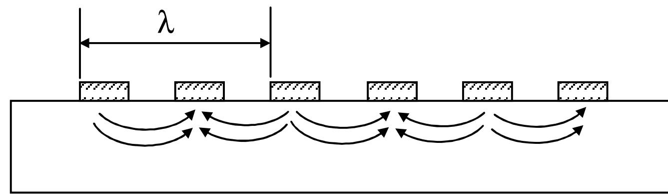

Figure 2.3 Electric field distributions of an IDT

produce a corresponding elastic strain distribution. When a sinusoidal voltage is applied, the elastic strains will oscillate with the applied voltage and each pair of electrodes can produce a SAW. If the applied voltage has a proper frequency of v/λ, where v is the SAW velocity in the substrate, and λ is the SAW wavelength, all the SAWs will have the same phase, i.e. these SAWs are constructive. This frequency is called the center frequency. Therefore, The IDT will output a maximum SAW and the SAW can travel across the device. If this SAW reaches another identical IDT on the substrate, it will be converted to voltage at the receiver IDT by piezoelectric coupling.

المنارة للاستشارات
www.manaraa.com

2.3.3 Electrode reflections of an IDT

The metal electrodes of an IDT will short the electric fields under them. This short condition will cause the discontinuity of SAW. Therefore, SAW will be reflected at the edge of the electrodes. For a uniform periodic IDT with single electrodes operating at the center frequency, the reflected SAWs at the edges of two adjacent electrodes have a phase shift of 2π, which means that the reflections will add in phase. Figure 2.4 schematically shows the reflections for a single-electrode IDT [5].

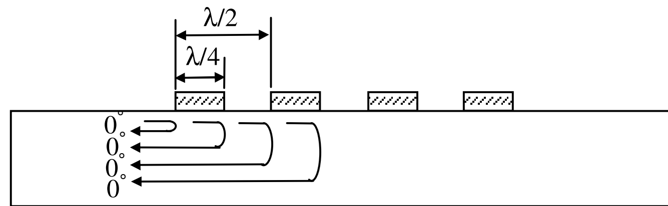

Figure 2.4 Reflections from the electrodes of a single finger IDT

In order to reduce the reflections from the electrodes, IDTs with double finger electrodes are typically used. Figure 2.5 shows the structure of a uniform periodic IDT with double finger electrodes. Unlike a single finger IDT, in the structure of a double finger IDT, the width of each electrode and the spacing between the adjacent two electrodes are λ/8, where λ is the SAW wavelength. Using double finger IDTs, The SAW reflections at the edges of two adjacent electrodes will have a phase shift of π at the center frequency, which means those reflections will cancel out, as shown in Figure 2.6 [5]. Although using a double finger IDT reduces the undesired reflections, it has a disadvantage of the requirement for a high resolution photolithography. Because the electrode width of a double finger IDT is half of that of a single finger IDT, in order to attain the same center frequency, the

المنارة للاستشارات
www.manaraa.com

photolithography resolution required for a double finger IDT must be twice of that for a single finger IDT.

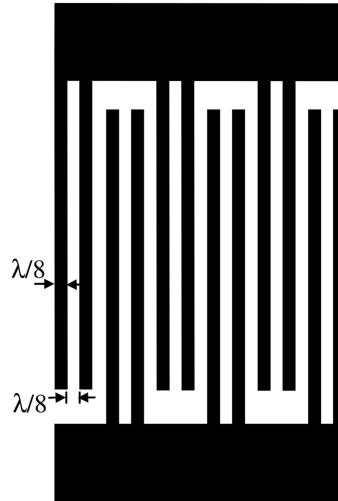

Figure 2.5 Structure of a uniform periodic IDT with double electrodes.

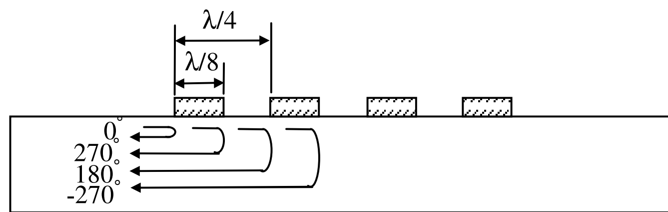

Figure 2.6 Reflections from the electrodes of a double finger IDT

www.manaraa.com

CHAPTER 3. THE FUNDAMENTALS OF ACT DEVICES

3.1 Basic ACT operations

As stated in a previous section, there is a traveling electric field associated with a SAW in a piezoelectric substrate. The electric field can act with the charges in a semiconductor layer on the substrate. An ACT device is a device that uses the electric field to bunch charges and transport them in the semiconductor layer.

The simplest type of ACT device is a delay line. Figure 3.1 shows schematically the cross section of an ACT delay line. When a high power SAW generated by an IDT propagates through the channel, an associated sinusoidal electric field generated by piezoelectric coupling will travel through the channel at the same speed and it causes a sinusoidal distribution of potential. Each trough of the potential can trap bunch electrons and transfer them through the channel.

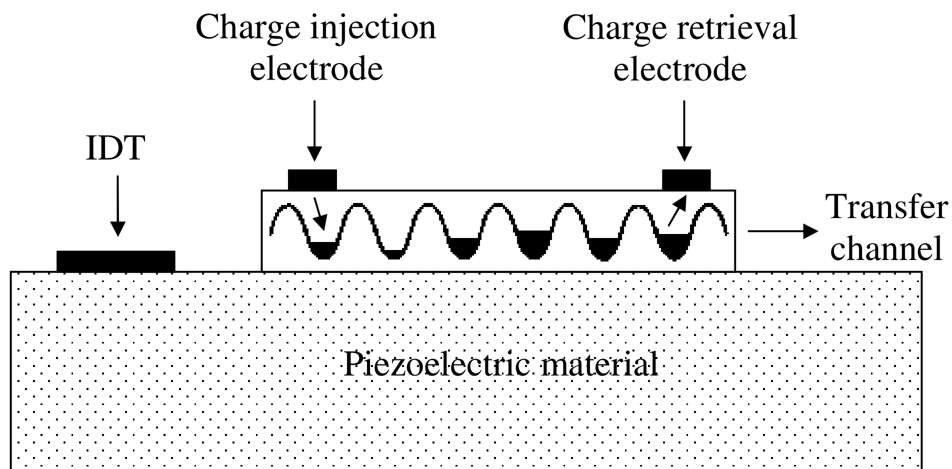

Figure 3.1 Schematic cross section of a basic ACT delay line.

المنارة للاستشارات
www.manaraa.com

Electrons can be injected into the channel by the input electrode. When the SAW passes the input electrode, the potential trough will pick off charges from the input contact. The amount of the charges in each potential trough is proportional to the voltage on the input electrode at the time the charges leave the electrode. Therefore, the SAW acts as a sampling mechanism in an ACT device and the amount of charges in the potential troughs will represent the variation of the input signal. Then these charge packets are transferred to the output electrode by the SAW and the charges in each potential trough will be retrieved there. Thus, the input signal will be restored on the output electrode.

3.2 SAW power requirements [17]

In order to transport the charge packets, the traveling electric field must be large enough to keep the charges confined. Therefore, a minimum value of the electric field amplitude E is required. The maximum electric field E can be written as

$$E = \frac{2\pi V}{\lambda}, \tag{3.1}$$

where λ is the SAW wavelength, and V is the amplitude of the piezoelectric voltage generated on the surface of a substrate by the SAW. According to Auld [18], V can be written as

$$V = \Phi_0 \sqrt{(P/A)/2\pi f}, \tag{3.2}$$

where Φ_0 is the normalized electric potential coefficient, f is the SAW frequency, P is the SAW power and A is the length of the transducer's acoustic aperture perpendicular to the SAW propagation direction. Substituting (3.2) into (3.1) gives

المنارة للاستشارات

www.manaraa.com

$$E = \frac{2\pi\Phi_0}{\lambda}\sqrt{(P/A)/2\pi f}\ . \quad (3.3)$$

According to (3.3), if a minimum value of the electric field E is required, the SAW power P also has a minimum requirement. This requirement is governed by two criteria.

First is the mobility criterion which requires that the carriers driven by the electric field must be able to move at the velocity of the SAW. This criterion can be expressed by the following equation as

$$E > v/\mu\ , \quad (3.4)$$

where v is the velocity of the SAW and μ is the carrier mobility in the semiconductor channel. Substitution of (3.4) into (3.3) yields

$$P/A > \frac{\lambda v^3}{2\pi\mu^2\Phi_0^2}\ , \quad (3.5)$$

which gives the minimum SAW power required per unit length acoustic aperture that can satisfy the first criterion.

Second is the thermal criterion which requires that the potential difference between SAW troughs and crests is much larger than the thermal energy so that the carriers will not diffuse between adjacent charge packets. The carriers are constrained in two dimensions. They are free in only one dimension. Therefore, the thermal energy will be ~k_BT, where k_B is Boltzmann's constant, and T is absolute temperature. Thus, this criterion requires V much greater than k_BT/e. If $V=10k_BT/e$ is taken for the purpose of the thermal criterion, the minimum SAW power required per unit length of acoustic aperture is

$$P/A = 2\pi f\left(\frac{10k_BT}{e\Phi_0}\right)^2, \quad (3.6)$$

المنارة للاستشارات
www.manaraa.com

3.3 Structures of charge transport channels in ACT devices

In an ACT device, a channel has to be formed so that the charges can be confined and transported in it. Currently, there are four ways to form a channel and confine charges in the channel.

1. Depletion layer [7]

Figure 3.2 shows the cross section of an ACT device with a depletion channel. The channel is formed by a Schottky-*N*-*P* layer geometry. When the *N* layer is biased with a high positive voltage, the whole *N* layer will be depleted. Thus, the electrons can be constrained in the *N* layer.

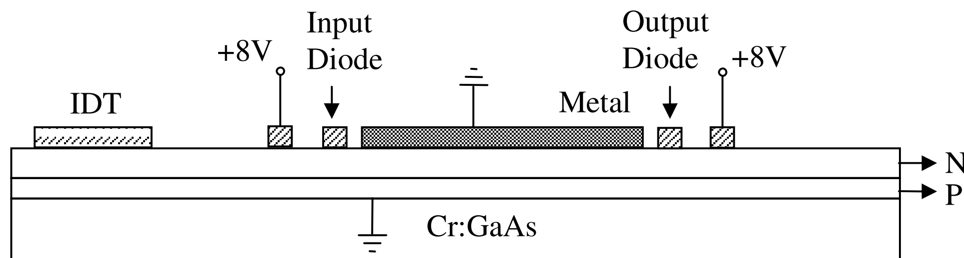

Figure 3.2 Cross section of an ACT device with a depletion channel [7].

2. Semiconductor thin film

In this structure, a semiconductor thin film is deposited on a piezoelectric substrate and is used as a charge transfer channel. The charge confinement in the vertical direction is achieved by the thin film itself. Figure 3.3 shows the cross section of this structure.

3. Quantum well [19]

The cross section of the quantum well structure is shown in Figure 3.4. A non-intentionally doped (NID) GaAs layer is placed between an *n*-AlGaAs layer and a NID

المنارة للاستشارات
www.manaraa.com

AlGaAs layer. Because of the energy band-gap differences and alignment of the conduction bands between the GaAs and AlGaAs, a potential well is formed in the GaAs layer. This well confines electrons in the direction normal to the surface of the material.

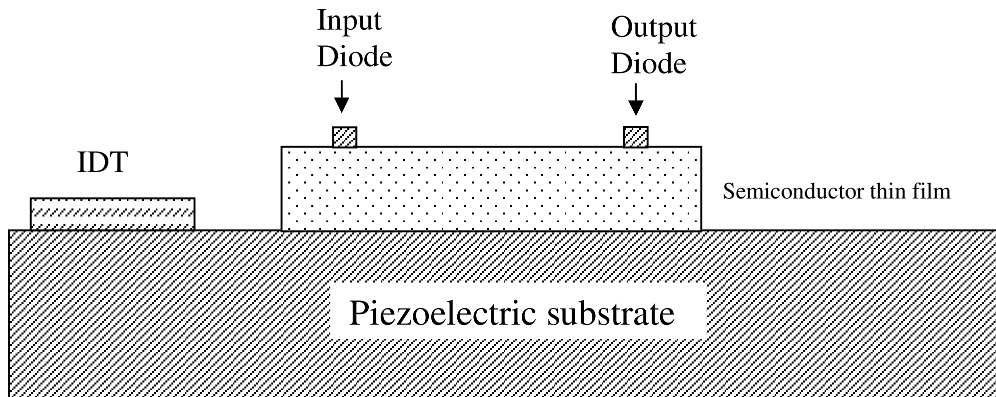

Figure 3.3 Cross section of an ACT with a thin film channel.

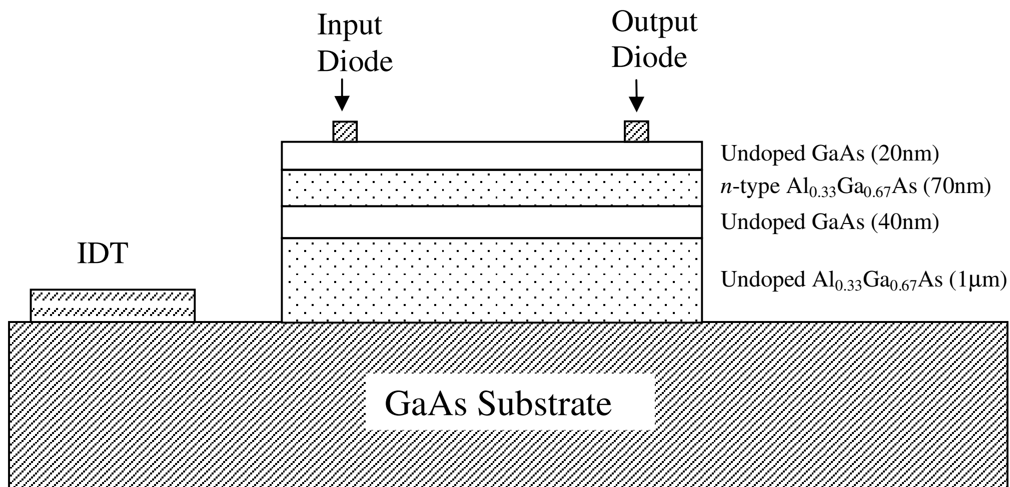

Figure 3.4 Cross section of an ACT with a quantum well channel [19].

4. Single heterojunction [20]

Unlike the quantum well structure which uses double-heterojunction, this structure uses only single heterojunction. Figure 3.5 shows its cross section. The electrons in the NID

المنارة للاستشارات
www.manaraa.com

GaAs layer are confined by the single heterojunction and the triangular potential created by the accumulated electrons.

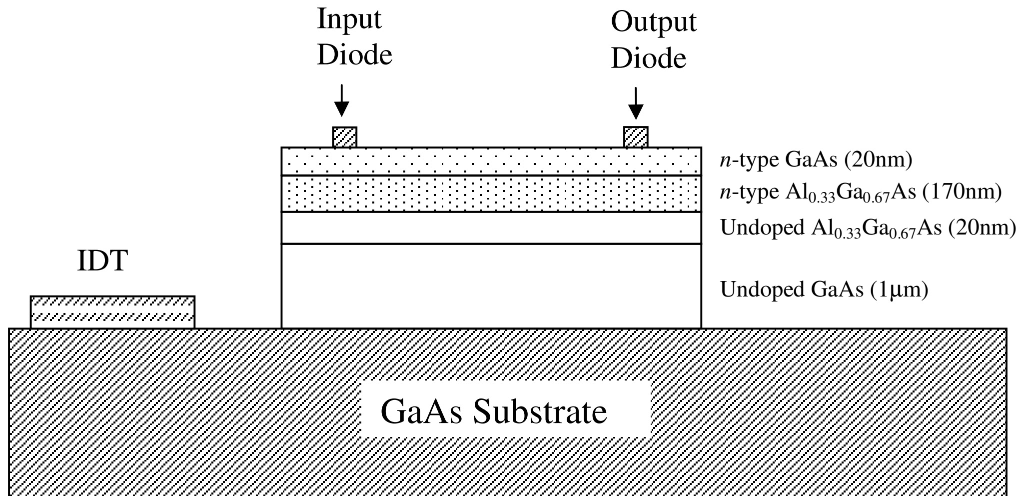

Figure 3.5 Cross section of an ACT device with a single heterojunction channel [20].

www.manaraa.com

CHAPTER 4. PIEZOELECTRIC COUPLING CONSTANT IN EPITAXIAL Mg-DOPED GaN

4.1 Introduction

Surface acoustic wave (SAW) devices are widely used in many applications, such as bandpass filters, radar systems, communication systems and nonlinear convolvers. Their working frequencies are usually from a few MHz to more than 1 GHz. Typically, SAW devices are made on quartz or $LiNbO_3$ because of their cost and excellent piezoelectric properties.

Although SAW devices using quartz and $LiNbO_3$ have proven highly successful, manufacturability would be considerably eased if SAW devices could be readily integrated with semiconductor devices. In a recent paper, Lee *et al.* [21] proposed Mg-doped epitaxial GaN as suitable for SAW devices integrated with other III-V materials. The electromechanical coupling factor (K^2), is one important parameter determining the acoustic behavior of a material. A large K^2 eases the design of wide-bandwidth low-loss SAW transducers. The piezoelectric constants are also of great interest in the design of strained-layer devices. For GaN doped with Mg at concentration $1.2\times10^{18}/cm^3$, Lee *et al.* [21] found $K^2 = (4.3 \pm 0.3)\%$, which is much higher than that of other III-V materials including undoped GaN. For example, GaAs has $K^2 = 0.04\%$ [18]; Woods & Boroumand [22] confirmed that (0001) orientation undoped GaN has $K^2 = (0.066\pm0.003)\%$ and O'Clock & Duffy [23] reported that $(11\bar{2}0)$ orientation undoped GaN has maximum $K^2 = 0.18\%$. If the high K^2 value [21] of Mg-doped GaN is confirmed, this would represent one of the highest values of

المنارة للاستشارات
www.manaraa.com

K^2 ever reported, and would revolutionize the design of acoustic devices integrated with III-V materials. Because of the importance of the large reported value [21] of this parameter for this material, K^2 was independently determined here using the same method as Lee *et al.* [21], but interpreting the results rigorously.

4.2 Experiment

4.2.1 Design of SAW filters

In order to determine the electromechanical coupling constant of an Mg doped GaN film, SAW filters were designed in this work. Each filter had two separated transducers and the separation between the transducers was 5mm. The surface acoustic wave propagates from one transducer to the other transducer along the $[\bar{1}100]$ direction of sapphire, which corresponds to the $[\bar{2}110]$ direction in GaN [24]. Double-finger IDTs were used to reduce the electrode reflections. Each IDT has 150 pairs of double-fingers. The width and spacing between the fingers were both λ/8 and the SAW aperture was 50λ, where λ is the wavelength of the SAW. According to O'Clock & Duffy [23], K^2 reaches its maximum when the GaN

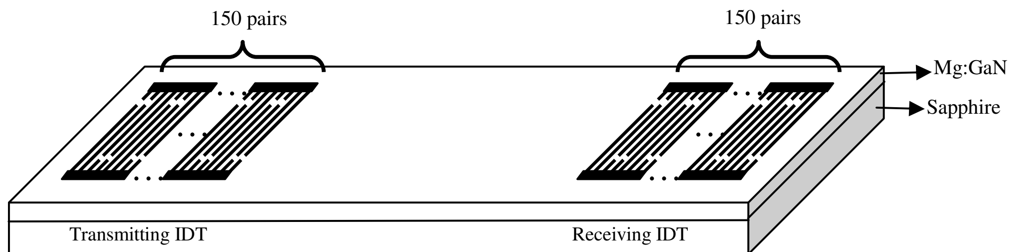

Figure 4.1 Schematic diagram of a SAW filter.

المنارة للاستشارات
www.manaraa.com

thickness-to-wavelength ratio is around 0.05. Therefore, IDTs having wavelengths of 32µm, 40µm, 48µm and 56µm were used in this work. This gives thickness-to-wavelength ratios of 0.0625, 0.05, 0.0417 and 0.0357, respectively. Figure 4.1 shows schematically the layout of a filter.

4.2.2 Fabrication of SAW filters

SAW filters were fabricated on an Mg doped GaN film using standard liftoff photolithographic techniques. The Mg doped GaN film ((0001) orientation) was grown by Technologies and Devices International, Inc., Silver Spring, MD, on a 2-inch *c*-plane sapphire substrate. The thickness of the GaN layer was 2µm. The concentration of Mg was $1.2\times10^{18}/cm^3$. The sheet resistance of the GaN layer was determined to be 2.5kΩ/□ using the Van der Pauw technique on a sample from the same wafer used for the acoustic tests. The contacts used in this measurement were palladium (20nm) on the material, capped by gold (230nm) for external connections, deposited by e-beam evaporation [25]. The resistivity in turn was calculated to be 0.5Ω·cm. The transducers were fabricated by evaporated aluminum and the thickness of the aluminum electrodes was 200nm. The measured DC resistance of the IDTs used was typically 100kΩ, indicating that good Schottky barriers were formed by the IDT metallization. All the fabrication process was done at Microelectronics Research Center (MRC). Detailed procedures are listed as following:

1. photoresist (AZ5209E) was spin coated at 4000 rpm for 40 seconds.
2. the samples were baked at 120^oC for 5 minutes on a hotplate.
3. the photoresist was exposed for 90 seconds using the MJB3 Karl Suss mask aligner.

المنارة للاستشارات

www.manaraa.com

4. the samples were develop for 60 seconds using AZ312 MIF developer (Dilution 1:1.2).
5. 200nm aluminum films were deposited on the samples using BJD1800 Temescal e-beam evaporator.
6. photoresist was removed from the samples using acetone.

After the fabrication, these devices were connected to BNC connectors using a wire bonder. A photograph of the final device is shown in Figure 4.2.

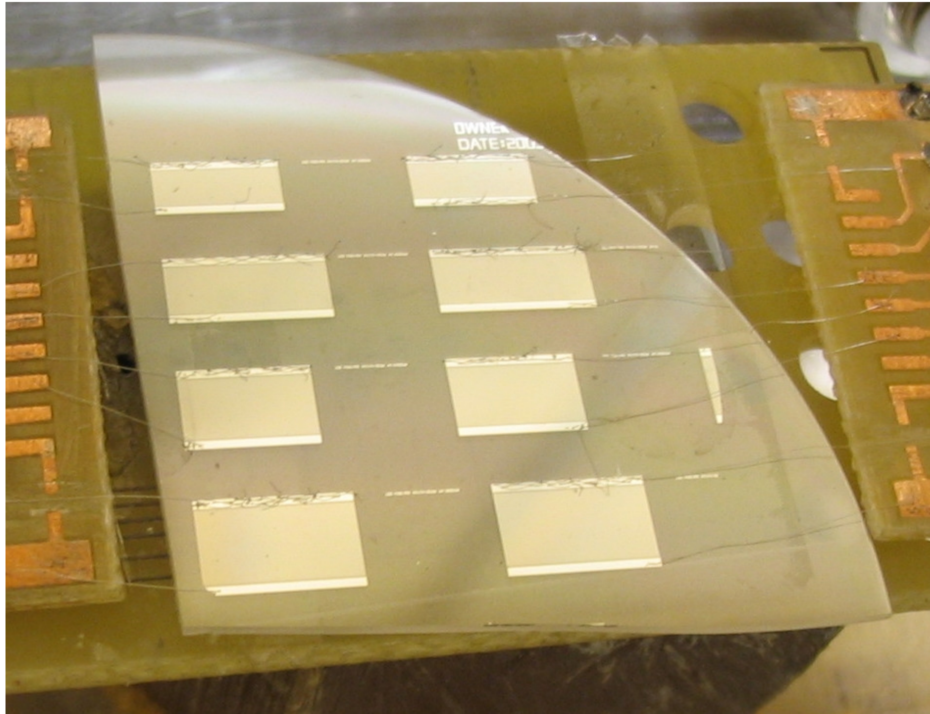

Figure 4.2 Photograph of the device.

4.2.3 Measurement

The time response of the SAW filters was measured by using a Textronix 2465B oscilloscope and the reflection coefficient for all devices was measured by a HP 8754A

www.manaraa.com

network analyzer. The experimental arrangement used to measure the time response of the SAW filters is shown schematically in Figure 4.3. The switcher used in this work comprised two Mini-Circuits ZP-5X frequency mixers connected in series and driven as simple on/off RF gates.

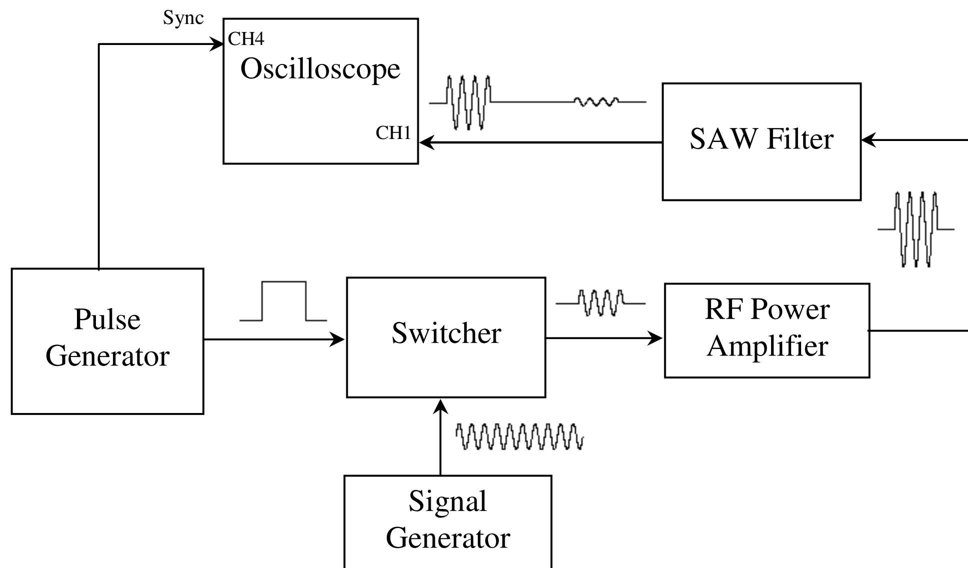

Figure 4.3 Schematic diagram of the experimental arrangement for time response measurement.

4.3 Results and Discussion

The electromechanical coupling factor K^2 can be calculated using the following equation given by Hartmann *et al.* [26]:

$$K^2 = \frac{G}{8 f_0 C_0 N}, \tag{4.1}$$

where G is the radiation conductance of the SAW IDT, f_0 is the center frequency, C_0 is the static capacitance of the IDT, and N is the number of finger pairs in the IDT.

المنارة للاستشارات
www.manaraa.com

However, Woods & Boroumand [22] found that when G is very small compared to the reactance of C_0, it is difficult to evaluate G accurately from static measurements of impedances from reflectivity measurements because the radiation effects are masked by stray capacitance. They pointed out that

$$G = \frac{|\delta\Re|}{2R_{in}}[1 + (R_p + R_{in})^2 \omega^2 (C_0 + C_p)^2], \quad \text{(for small } G \text{ only)} \tag{4.2}$$

where $\delta\Re$ is the change in reflection coefficient at center frequency with and without the radiation conductance present, R_{in} is the source impedance, and C_p is the capacitance of the device package.

Therefore, G can be evaluated by measuring $\delta\Re$. In principle, $\delta\Re$ can be measured by a network analyzer [22], as shown in Figure 4.4.

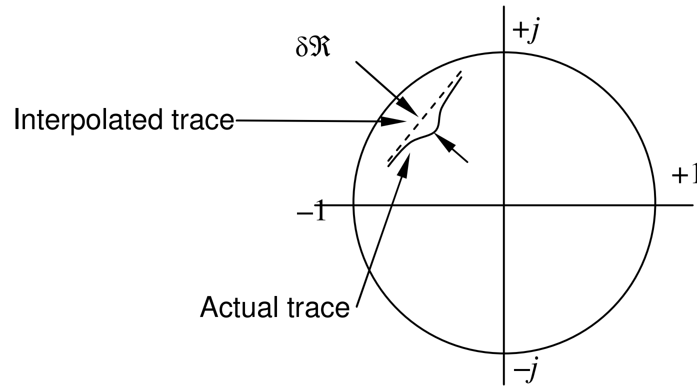

Figure 4.4 A typical Smith chart of reflection coefficient for an interdigital transducer [22].

However, in the present work, $\delta\Re$ for all devices was too small to be measured, as shown in Figure 4.5. On the screen of the network analyzer, no change of the reflection

المنارة للاستشارات
www.manaraa.com

coefficient can be seen for any devices around the center frequencies. This indicates that G is very small. Therefore, it is impossible to use (4.1) to calculate K^2.

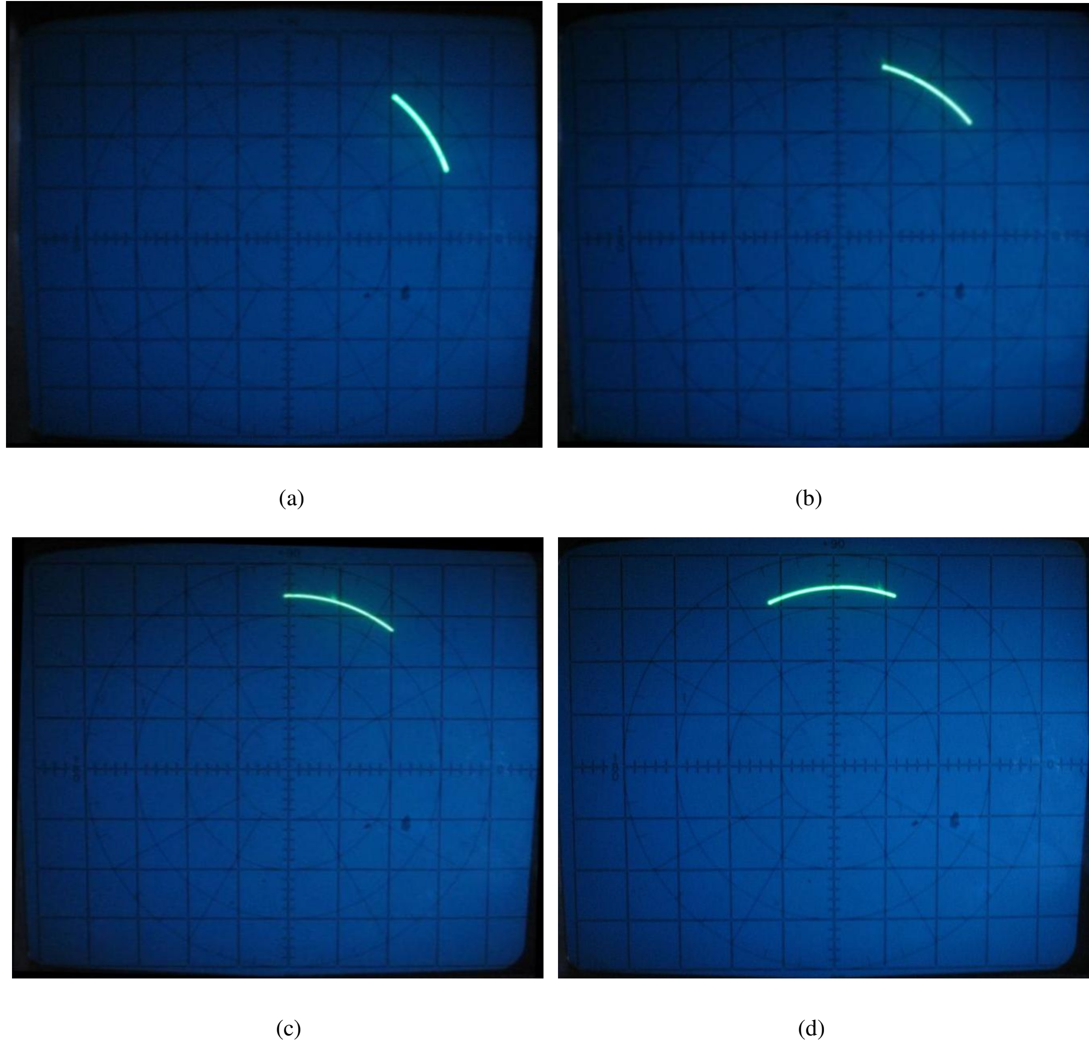

(a) (b)

(c) (d)

Figure 4.5 Smith chart of reflection coefficient for all devices. (a) device wavelength 32µm, (b) device wavelength 40µm, (c) device wavelength 48µm, (d) device wavelength 56µm.

Another way to evaluate K^2 is to measure the insertion loss of a SAW filter. Using the equivalent circuit model of an IDT given by Hartmann *et al.* [26], at center frequency the acoustic susceptance B is zero [26], so that the equivalent circuit is that shown in Figure 4.6.

المنارة للاستشارات
www.manaraa.com

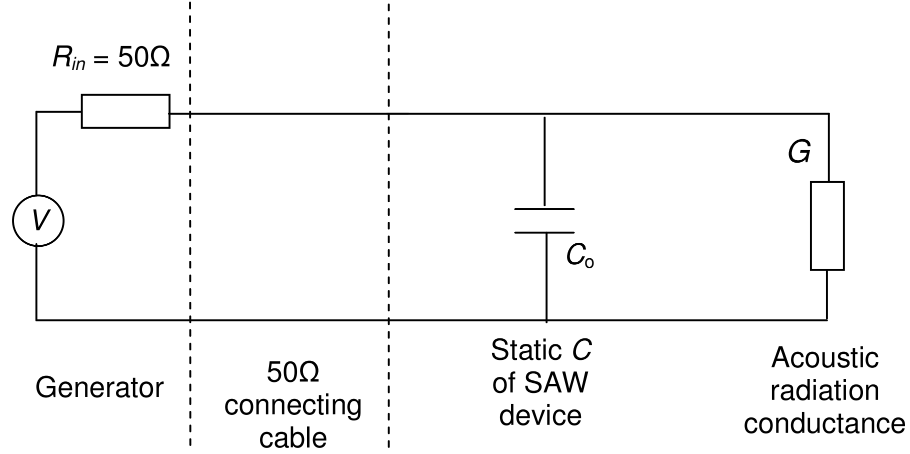

Figure 4.6 Simple equivalent circuit model used to estimate the IDT transduction loss.

Since only half of the radiated SAW power propagates directly to the receiver IDT, the insertion loss of a single IDT is then

$$\left| \frac{G/2}{[R_{in}(G + j\omega C_0) + 1](G + j\omega C_0)} \right|. \tag{4.3}$$

For the present devices, $G << \omega C_0$ and $R_{in}\omega C_0 << 1$, so that the insertion loss of one IDT can be reduced to

$$\frac{G}{\omega C_0} = \frac{2K^2 N}{\pi}. \tag{4.4}$$

Since the propagation loss in a sapphire substrate is very small, it can be ignored. The insertion loss of a SAW filter using two IDTs is then

$$\left(\frac{2K^2 N}{\pi} \right)^2. \tag{4.5}$$

Therefore, once the insertion loss of a SAW filter is measured, K^2 can be calculated from equation (4.5). In the presented work, the insertion loss of a SAW filter was measured

المنارة للاستشارات
www.manaraa.com

from the time response of that filter. Figure 4.7 shows the time response of each of the four devices to an RF pulse. No output signal was detected for the device having $\lambda = 32\mu m$. For the other three devices, weak output signals were detected. A drop of water placed between the transducers of each device severely attenuated the output signal after the breakthrough burst pulse, which showed that the output signal was produced by a surface acoustic wave. The frequencies of the acoustic burst pulse signals at maximum received acoustic amplitude were 136.09MHz, 114.48MHz and 98.64MHz, respectively. Therefore, the velocity of the surface acoustic wave is around 5500m/s under the transducers, which agrees with the result given by O'Clock & Duffy [23]. Since the space between the two transducers of each device is 5mm, the time delay is about 1μs as shown in Figure 4.7.

The insertion loss of a SAW filter can be measured by replacing that filter with an attenuator and comparing the amplitude of the attenuator output signal to the amplitude of the acoustic burst pulse signal through the filter. In the presented work, the insertion loss of each SAW filter was measured to be higher than 80dB. Hence, the electromechanical coupling factor K^2 of the Mg-doped GaN epilayer was less than $1\times10^{-4}\%$. This is extremely small compared to the value $K^2 = (4.3 \pm 0.3)\%$ reported by Lee *et al.* [21]. This value is also much smaller than the value $K^2 = (0.066\pm0.003)\%$ given by Woods & Boroumand [22] for undoped GaN. Our lower value shows that the Mg-doped GaN epilayer does not appear to be a practical material for SAW devices.

المنارة للاستشارات

www.manaraa.com

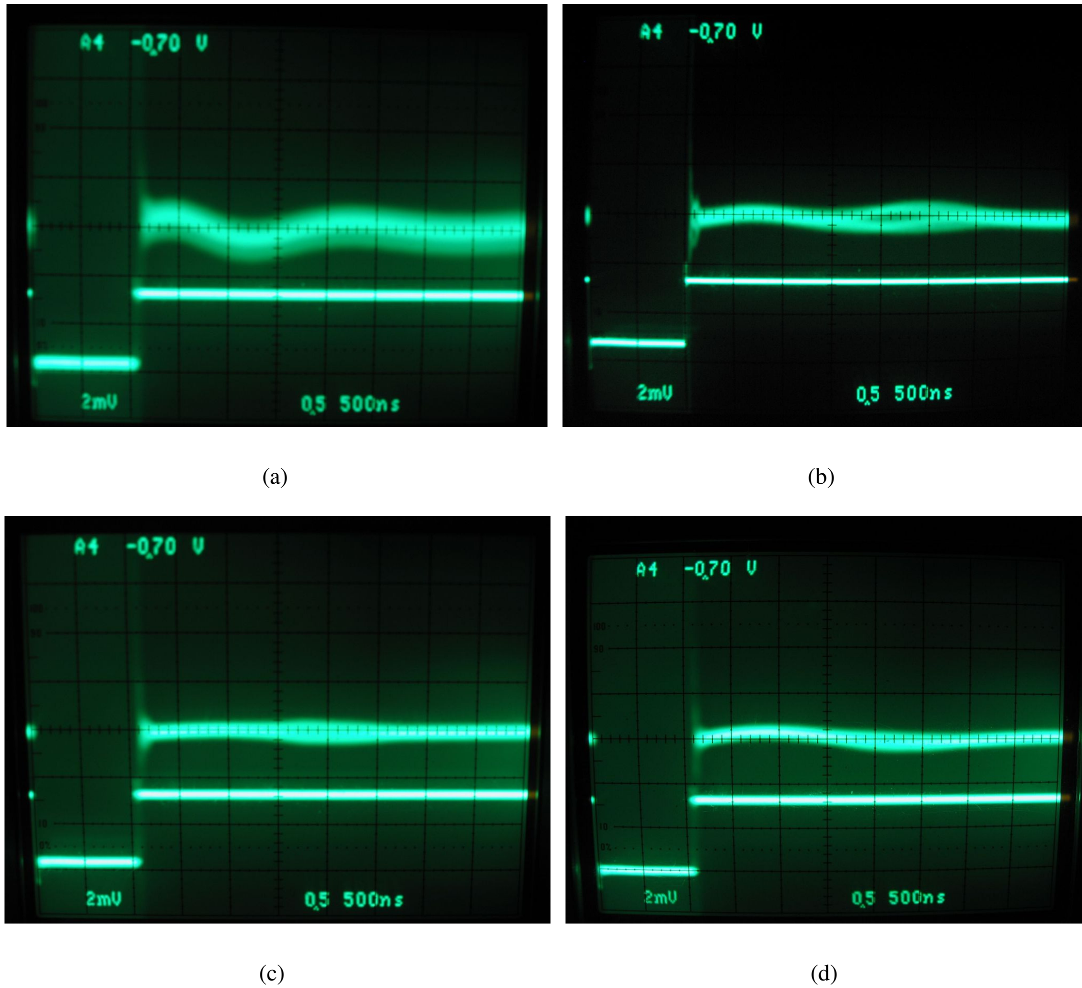

(a) (b)

(c) (d)

Figure 4.7 Time response of SAW filters to an RF pulse. Horizontal axis: 500ns/div; vertical axis: voltage (arbitrary units). In each case, the received acoustic pulse starts ~2 horizontal divisions after the end of the launching RF pulse and is comparable with system noise. Acoustic wavelength (a) 32µm, (b) 40µm, (c) 48µm, (d) 56µm.

4.4 Conclusions

SAW filters were fabricated on an Mg-doped GaN epilayer grown on a sapphire substrate. For devices having λ = 40µm, 48µm and 56µm, very weak output signals were detected in the measurement of their time response to an RF signal at center frequencies of 136.09MHz, 114.48MHz and 98.64MHz respectively. No change of the reflection coefficient was detectable using the available network analyzer for all devices around the center

المنارة للاستشارات

www.manaraa.com

frequencies. The insertion loss for all devices was higher than 80dB. Detailed equivalent-circuit analysis of the insertion-loss results, taking complete account of the test fixture impedance, stray capacitance, and other electrical properties, which appears not to have been done by the original authors [21], shows that K^2 for the Mg-doped GaN epilayers has an upper bound of ~0.0001%. This is extremely small, much less than other III-V materials, and so this material does not appear to be as promising for SAW applications as was claimed by Lee *et al.* [21]. The IDT DC resistance was much larger than the system RF characteristic impedance although the layer resistivity was quite low, indicating that good Schottky contacts were maintained and also indicating that the Mg dopant may have been activated in the sample used, even though it had not been annealed after deposition.

المنارة للاستشارات
www.manaraa.com

CHAPTER 5. DESIGN OF PENTACENE ACOUSTIC CHARGE TRANSFER DEVICES

5.1 Introduction

Acoustic charge transfer (ACT) devices are based upon moving charges in a semiconductor using surface acoustic waves. They are promising devices for building powerful analog signal processors which will have many applications in both defense and commercial areas. Because of the properties of high processing speed, small size, light weight and low power consumption, they will have many applications, including innovative modems, channel simulators, video and IF preprocessors and receiver post-processors for communications, radar, electronic warfare, and instrumentation systems [12].

In order to move charges, a charge transfer channel must be defined in an ACT device. The formation of channels in current ACT devices involves epitaxial layers of III-V semiconductors. For example, Hoskins *et al.* [7] used Schottky-N-P layer geometry to form a channel; Tanski *et al* [19] demonstrated an (Al,Ga)As/GaAs/(Al,Ga)As heterojunction channel; Hayden *et al* [20] reported an (Al,Ga)As/GaAs single heterojunction ACT device. However, growing epitaxial layer for III-V semiconductors needs expensive deposition techniques, such as MOCVD and MBE. In this work, a new ACT device was designed using organic semiconductor pentacene as a charge transfer channel which can be easily formed by thermal evaporation so that the low fabrication cost can be exploited in an ACT device. That will make ACT devices more attractive.

المنارة للاستشارات

www.manaraa.com

5.2 Design of acoustic charge transfer devices using pentacene [17]

The goal of this novel ACT is to use pentancene as a charge carrier transfer channel. The pentacene will be deposited along the SAW propagation track on a piezoelectric substrate. The charge confinement in vertical direction is achieved by the pentacene layer itself. However, the carrier mobility in pentacene is very small, about $10^{-4}m^2V^{-1}s^{-1}$ [27]. According to (3.5), if the SAW wavelength is 12μm and the SAW propagates along Z direction in a Y-cut $LiNbO_3$ substrate, i.e. v=3487.7m/s [18] and Φ_0=14500$Vm^{1/2}J^{-1/2}$ [18], the minimum requirement for the SAW power per unit length of acoustic aperture is $3.86\times10^4Wm^{-1}$. If bidirectional IDTs are used and the IDTs are operated matched, the minimum electrical power input required per unit length of acoustic aperture is twice of the SAW power requirement, i.e. $7.72\times10^4Wm^{-1}$. For a typical simple SAW transducer aperture of 0.5mm, this corresponds to 38.6W electrical drive, which is too high for efficient practical operation. Since the power requirement is proportional to v^3, a substantial reduction in power requirement may be expected for substrates having low SAW velocity. Of all the commonly available SAW substrates, $Bi_{12}GeO_{20}$ has by far the lowest SAW velocity. Therefore, it is the most attractive substrate in this application. However, even if a $Bi_{12}GeO_{20}$ substrate is used, the required electrical drive is still as high as 10.9W.

To further reduce the required electrical drive power, a SAW beam compressor will be used which can focus down a large aperture of SAW produced by an IDT to a narrow guilded-beam acoustic track. This technique has been used for many years in $LiNbO_3$ SAW convolvers so that a high SAW power density could be achieved to enhance the non-linearity. Several ways have been used to compress SAW beamwidth, including thin-film metalized

المنارة للاستشارات

www.manaraa.com

straight edge horn [28], thin-film metalized parabolic horn [29], multistrip coupler [30], and chirped IDTs [31]. All these methods have proven highly successful in improving the SAW power density. After the comparison of their advantages and disadvantages, as shown in Figure 5.1, the parabolic metalized horn design was finally chosen. By such a horn the SAW beam will be compressed to around 3λ aperture in order to obtain a high acoustic power density and avoid the multimoding effect [32]. Using a beam compressor can reduce the required minimum electrical drive power for a $LiNbO_3$ and a $Bi_{12}GeO_{20}$ substrate to 2.78W and 0.78W, respectively.

	Advantages	Disadvantages
Straight Edge Horn	Very easy to design	Compressor is long Severe mode coupling problem
Parabolic Horn	Easy to design	Compressor is long
Multistrip Coupler	Easy to design Compressor is short	Require high-resolution photolithography to fabricate.
Chirped IDTs	No need of compressor	Hard to design

Figure 5.1 A comparison of the advantages and disadvantages of different beam compression methods

After the SAW beam being compressed to 3λ aperture, a topographic waveguide will be used to prevent the compressed SAW beam from diffracting to much larger apertures. In order to form a topographic waveguide, a mass will be deposited on the surface of a substrate and the deposited material must be able to cause a reduction of the SAW velocity as required to guide SAW. For an isotropic substrate, the change of the SAW velocity caused by the extra mass is given by [18]

المنارة للاستشارات

www.manaraa.com

$$\frac{\Delta v}{v} = \left(\frac{vh}{4}\right)\left[\rho^{'}\frac{|v_{\perp}|^2}{(P/A)} + \left(\rho^{'} - \frac{4c_{44}^{'}}{v^2}\cdot\frac{c_{12}^{'}+c_{44}^{'}}{c_{12}^{'}+2c_{44}^{'}}\right)\frac{|v_{\parallel}|^2}{(P/A)}\right], \tag{5.1}$$

where h is the layer thickness (small compared to a SAW wavelength), $\rho^{'}$ is the mass density of the deposited material, $v_{\perp}$ and $v_{\parallel}$ are the perpendicular and tangential surface particle velocities respectively, P/A is the acoustic SAW power per unit acoustic aperture length, and $c_{12}^{'}$ and $c_{44}^{'}$ are the elastic constants of the deposited material. If the deposited material can cause a positive $\Delta v/v$, then it can be used for a topographic waveguide. Fortunately, Pentacene is such a material that will cause a positive $\Delta v/v$. Therefore, the pentacene charge transfer channel in this design will also be used as a topographic waveguide.

Since the elastic constants of thin-film pentacene or similar materials do not appear to have been reported previously, the accurate value of $\Delta v/v$ is unable to be calculated. However, an estimate value can be given using the parameters of a similar material. Among all the organic materials which have elastic constants listed in Reference [33], naphthalene has the largest $c_{44}^{'}$, which is $330\times10^{6}\text{Nm}^{-2}$. Using this value gives an estimate of $\frac{4c_{44}^{'}}{v^2} \approx 453\,\text{kgm}^{-3}$ for a $Bi_{12}GeO_{20}$ substrate. Therefore, the adjustment term $\frac{4c_{44}^{'}}{v^2}\cdot\frac{c_{12}^{'}+c_{44}^{'}}{c_{12}^{'}+2c_{44}^{'}}$ is rather less than 453kgm^{-3}. In a first approximation, 453kgm^{-3} will be used as the adjustment term. Thus, (5.1) can be written as

$$\frac{\Delta v}{v} = \left(\frac{vh}{4}\right)\left[\rho^{'}\frac{|v_{\perp}|^2}{(P/A)} + (\rho^{'} - 453)\frac{|v_{\parallel}|^2}{(P/A)}\right]$$

المنارة للاستشارات

www.manaraa.com

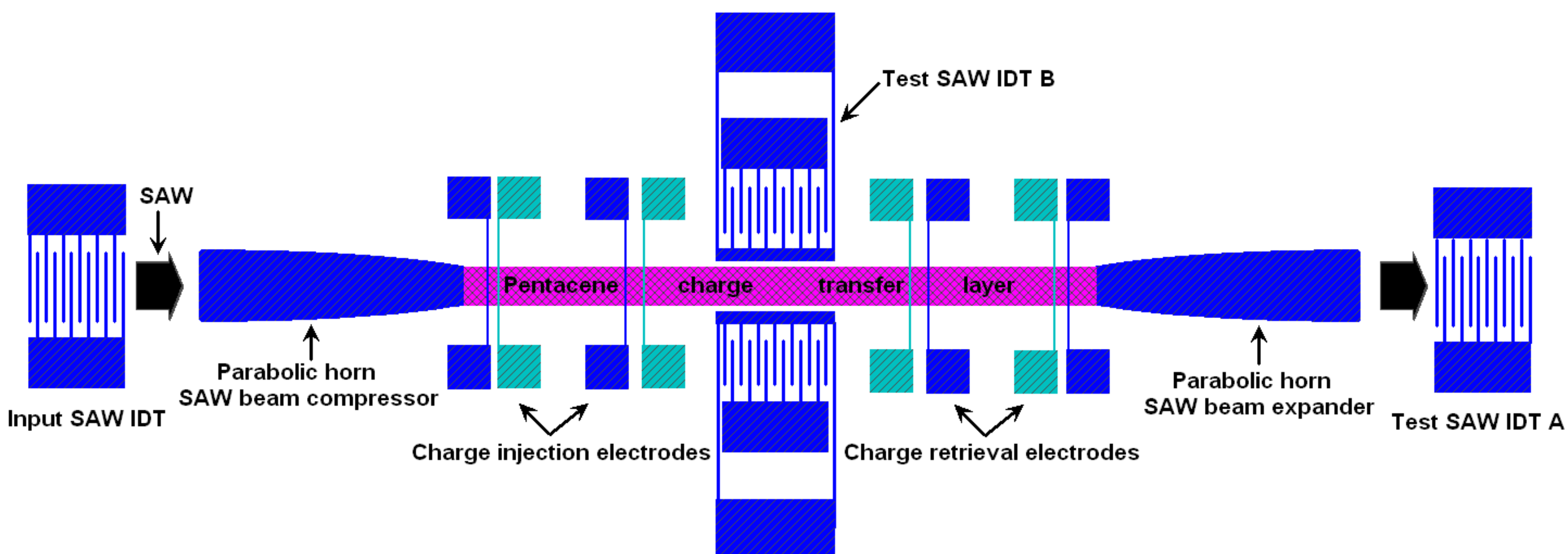

Figure 5.2 Plan view of pentacene ACT configuration.

المنارة للاستشارات
www.manaraa.com

The quantities $\frac{|v_\perp|^2}{(P/A)}$ and $\frac{|v_\parallel|^2}{(P/A)}$ are tabulated by Auld [18] for a number of materials, including $Bi_{12}GeO_{20}$. Using the values h=1µm, ρ'=1300kgm^{-3} [34], and λ=12µm, gives

$$\frac{\Delta v}{v} \approx 0.0086 \tag{5.2}$$

The final design of a pentacene ACT (PACT) device is shown in Figure 5.2, in which the IDT produces the SAW; the beam compressor is used to compress the SAW beam to reduce the minimum requirement of the electrical drive power; the pentacene layer is used as a charge transfer channel and a SAW waveguide; and the injecting and retrieving electrodes are used to inject and retrieve charges.

5.3 Design of a parabolic SAW beam compressor

Since the shape of the compressor is determined to be a parabolic horn, the key point of the design is to obtain the parabola equation. This can be easily done using ray optics.

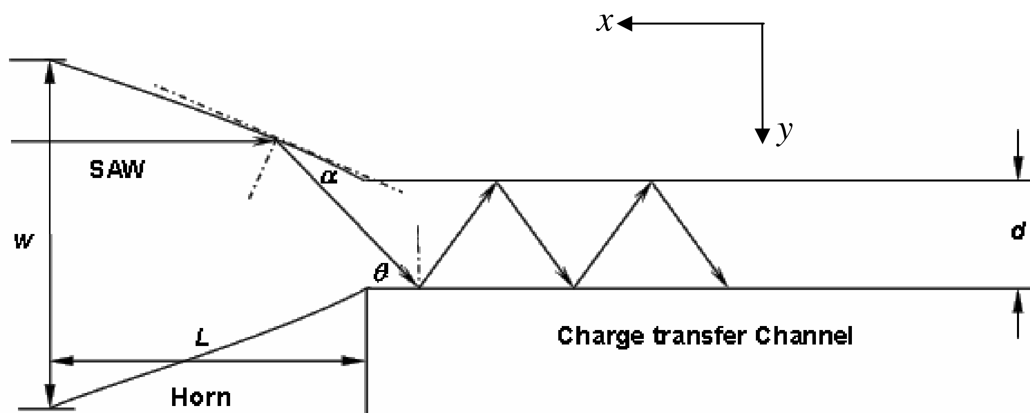

Figure 5.3 Geometry of beam compressor.

المنارة للاستشارات
www.manaraa.com

Figure 5.3 shows the reflection of a surface acoustic beam in a parabolic compressor and a waveguide. Within the horn and the waveguide, the SAW velocity (v_{in}) is less than the velocity (v) outside the horn and the waveguide. The guiding action is achieved by total internal reflection of the SAW beam at the interfaces between the slow and fast regions. From Snell's law in optics, the critical angle θ_c is defined as

$$\theta_c = \cos^{-1}\frac{v_{in}}{v}$$

Thus,

$$\cos\theta_c = \frac{v_{in}}{v} = 1 - \frac{\Delta v}{v},$$

where $\Delta v = v - v_{in}$. Referring to Figure 1, the relation between the horn taper angle α and the zigzag angle θ is easily found from geometry as

$$\theta = 2\alpha$$

The SAW beam suffers a total internal reflection when $\theta \leq \theta_c$. Therefore,

$$\cos\theta \geq \cos\theta_c = 1 - \frac{\Delta v}{v}$$

$$\cos 2\alpha \geq 1 - \frac{\Delta v}{v}. \qquad (5.3)$$

According to double-angle formulae,

$$\cos 2\alpha = 1 - 2\sin^2\alpha. \qquad (5.4)$$

Substituting (5.4) into (5.3) gives

$$1 - 2\sin^2\alpha \geq 1 - \frac{\Delta v}{v}$$

المنارة للاستشارات

www.manaraa.com

$$\sin\alpha \le \left(\frac{\Delta v}{2v}\right)^{1/2}$$

Since α is very small,

$$\alpha \approx \sin\alpha \le \left(\frac{\Delta v}{2v}\right)^{1/2} \qquad (5.5)$$

For a parabolic horn beam compressor, the taper angle is smallest at the widest part of the horn and is largest at the narrowest part of the horn. Therefore, if the largest taper angle satisfies (5.5), then all the taper angles will satisfy (5.5). To simplify the calculation, assume the parabola equation is

$$x = py^2,$$

where p is a constant. Thus, the largest taper angle $\alpha_{\max}$ is

$$\alpha_{\max} = \tan^{-1}\left(\frac{1}{pd}\right) \approx \frac{1}{pd}, \qquad (5.6)$$

where d is the width of the waveguide. To make $\alpha_{\max}$ satisfy (5.5), p has to satisfy

$$\frac{1}{pd} \le \left(\frac{\Delta v}{2v}\right)^{1/2}$$

$$p \ge \frac{1}{d}\left(\frac{\Delta v}{2v}\right)^{-1/2}. \qquad (5.7)$$

To minimize the length of the parabolic horn, the minimum value of p is taken. Thus, the parabola equation is then

$$x = \left[\frac{1}{d}\left(\frac{\Delta v}{2v}\right)^{-1/2}\right]y^2$$

The length of the parabolic horn in turn is

المنارة للاستشارات
www.manaraa.com

$$L = \frac{d}{4}\left(\frac{\Delta v}{2v}\right)^{-1/2}\left[\left(\frac{w}{d}\right)^{2} - 1\right]. \quad (5.8)$$

If the compression ratio *CR* is defined as

$$CR = w/d\,,$$

(5.8) can be written as

$$L = \frac{d}{4}\left(\frac{\Delta v}{2v}\right)^{-1/2}\left[CR^{2} - 1\right]$$

which is in agreement with the length given by Malocha [35].

In this design, d=36μm, which is equal to three SAW wavelengths. According to (5.2), $\Delta v/v$ is approximately equal to 0.0086 for a 1μm-thick pentacene layer on a $Bi_{12}GeO_{20}$ substrate. However, there is a large uncertainty and the actual $\Delta v/v$ value might be less than 0.0086. According to (5.7), the $\Delta v/v$ value used to design the compressor should be equal to or less than the actual value. Therefore, a value of $\Delta v/v$=0.007 which is a little bit less than 0.0086 was chosen to design the compressor. From (5.1), it is seen that the actual $\Delta v/v$ value can be adjusted by the thickness of the pentacene layer. So, even the $\Delta v/v$ value fixed on the mask didn't satisfy (5.7) for a 1μm-thick pentacene layer, the final thickness of the pentacene layer might increase to make the actual $\Delta v/v$ value greater than 0.007. The choice of *CR* was a tradeoff between the IDT aperture and the compressor length. For the IDT, a large *CR* is desired for a large aperture to reduce beam steering and diffraction [16]. For the compressor, a small *CR* is expected for a short length. Finally, *CR*=10 was chosen in this work to give a 30-wavelength IDT aperture and a 1.506cm compressor so that the whole device could be

المنارة للاستشارات
www.manaraa.com

fabricated on a 2-inch wafer. Thus, the parabola equation for the compressor in this work is then

$$x = 0.469 y^2 \qquad (5.9)$$

5.4 Design of masks

The whole ACT device was defined by three masks. Mask 1 defined the IDTs, parabolic horn SAW beam compressor, and Schottky electrodes. The input IDT was made of 15 pairs of single fingers. The width of each finger and the spacing between two adjacent fingers were 3μm. Thus, the SAW wavelength was 12μm. The aperture of the input IDT was 360μm which is 30 times of the SAW wavelength. The edge of the parabolic horn was determined by (5.9). In this design, the parabolic compressor was approximated by 500 trapezia which evenly divided the compressor along the x axis. It is easy to show that this approximation only gives a maximum error of 0.01μm which is far beyond the resolution of the mask aligner at MRC. Therefore, these trapezia were good enough to describe a parabolic horn. The width of the Schottky electrodes was 3μm. Mask 2 defined the Ohmic electrodes and bonding pads. The width of the Ohmic electrodes was also 3μm. An Ohmic electrode and a Schottky electrode will form an input or output diode. The spacing between the two electrodes changed from 3μm to 12μm so that an input signal could be processed in different ways. Mask 3 defined the pentacene charge transfer channel. The width of the channel was 36μm and the length is 6mm. In order to generate the patterns of these parts, a small SKILL program was written and run in Cadence. After that, a number of alignment marks were put on each mask. Each alignment mark consisted of four crosses with different sizes.

المنارة للاستشارات
www.manaraa.com

5.5 Distillation of pentacene

5.5.1 The reasons of pentacene distillation

It was reported [36] that the impurities in pentacene can decrease the hole mobility in pentacene. According to (3.5), the minimum power requirement is inversely proportional to μ^2. Thus, increasing the hole mobility in pentacene can greatly reduce the required SAW power. However, Pentacene purchased from Aldrich only has a purity of 97%. It contains nonnegligible amounts of 6,13-dihydropentacene (DHP), 6,13-pentacenequinone (PQ), aluminum, and iron [37]. Therefore, it is important to purify pentacene. The purification is generally done by sublimation in a temperature gradient furnace. Since impurities and pentacene have different sublimation temperatures, they will deposit and be separated in different temperature zones in a gradient furnace. Thus, impurities can be removed from pentacene.

5.5.2 The design of a temperature gradient furnace

In the present work, a temperature gradient furnace was designed. The schematic of the temperature gradient furnace is shown in Figure 5.4. The whole furnace consisted of a quartz source tube, a pyrex crystal growth tube, a quartz reactor tube and a pyrex insulation tube, the sizes of the tubes [37] are shown in Figure 5.4. A Nickel-Chromium alloy heating wire was used to heat the furnace.

In this design, the determination of the heating wire model is important. Reference [38] describes how to design a heating coil for a furnace.

The power needed to heat the furnace can be calculated by

$$P = \frac{W_T C_P \Delta T}{3412 \times t},$$

www.manaraa.com

where P is the power in kW, W_T is the weight of the furnace material in lb, C_P is the specific heat of the furnace material in BTU/lb·°F, ΔT is the temperature difference in °F, and t is the time allowed for heat-up time in hr. In the present work, a quartz reactor tube was used as a furnace, and a quartz source tube and a pyrex crystal growth tube were also heated. The sizes of the tubes were shown in Figure 5.4. In order to simplify the calculation, the mass density and the specific heat of quartz were used for all the three tubes in the following calculation.

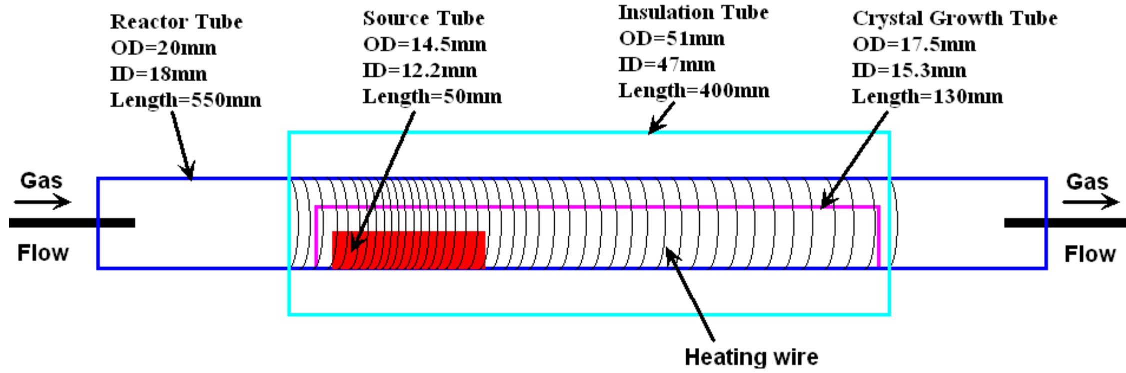

Figure 5.4 Schematic diagram of a temperature gradient furnace

Therefore, the weight of the material heated is

$$W_T = \rho V$$

where ρ is the mass density of the heated material, V is the volume of the material. Using the sizes of the tubes, V is calculated to be

$$V = \frac{1}{4}\pi\left[\left(0.02^2 - 0.018^2\right)\times 0.4 + \left(0.0145^2 - 0.0122^2\right)\times 0.05 + \left(0.0175^2 - 0.0153^2\right)\times 0.13\right]$$

$$=0.3365\times 10^{-4}\ \mathrm{m}^3.$$

The density for quartz is 138lb/ft^3 [38], which is equal to 2211kg/m^3. Therefore, the weight of the three tubes is

المنارة للاستشارات
www.manaraa.com

$$W_T = 2211\times0.3365\times10^{-4} = 0.0744 \text{ kg} = 0.164 \text{ lb}$$

The specific heat of quartz is 0.26BTU/lb·°F [38]. According to [37], the distillation temperature is better under 300°C to avoid any residue or byproducts. However, in this design, a temperature of 450°C which is equal to 800°F was used to give a large margin for possible future uses. Thus, if assume that the temperature is even all over the furnace, and the room temperature is 70°F, the temperature difference is then

$$\Delta T = 800 - 70 = 730\,°\text{F}$$

If the heat-up time t=0.08hr, the power needed for heating up the tubes is

$$P = \frac{0.164\times0.26\times730}{3412\times0.08} = 0.114 \text{ kW}$$

The power loss from the surface due to convection and radiation can be calculated from the heat loss curve. However, the heat loss curve for quartz is not provided by this reference. In order to estimate the power loss, a value of 600W/ft^2 for oxidized aluminum at 800°F [38] is used here. The surface area of the furnace is

$$\pi\times0.02\times0.4\times2 = 0.0503 \text{ m}^3 = 0.5414 \text{ ft}^2.$$

Therefore, the power loss is

$$P_{loss} = \frac{600\times0.5414}{1000}\times0.83 = 0.27 \text{ kW},$$

where a factor of 0.83 is multiplied since the furnace is a horizontal pipe [38].

For start-up operations, the required power is [38]

$$P_{start} = (P + 2P_{loss}/3)\times1.15 = 0.338 \text{ kW}$$

For sustained operations, the required power is [38]

$$P_{sustain} = P_{loss}\times1.15 = 0.31 \text{ kW}$$

المنارة للاستشارات
www.manaraa.com

Therefore, the start-up is the governing power for this furnace. Since the furnace is heated by a resistance heating wire, the resistance must satisfy

$$R \le \frac{U^2}{P_{start}} = \frac{110^2}{0.338 \times 1000} = 35.8 \ \Omega,$$

where U is the voltage applied to the furnace.

Assume that there is a turn of heating wire every half centimeter along the furnace, so there are a total of 80 turns of the heating wire. The total length of the heating wire is then

$$80 \times \pi \times 0.02 = 5.03 \text{ m} = 16.5 \text{ ft}$$

Therefore, the resistance per unit length will be less than

$$35.8 / 16.5 = 2.17 \ \Omega/\text{ft}$$

The closest Omega heating wire model that satisfies the above requirement is NI80-020 which has the resistance per unit length of 1.72Ω/ft at 800°F.

After the heat wire was wrapped on the reactor tube, it was connected to an autotune PID (proportional, integral, derivative) temperature controller (Omega CN77333) which has a high accuracy of ±0.5°C. The source temperature was regulated by the controller through a thermocouple (Omega TJC36-CASS-032G-18-SMP-M). This thermocouple has a stainless steel sheath to give minimum contamination to the pentacene.

5.5.3 Operation of the furnace

Pentacene was placed in the source tube, the source tube was placed inside the crystal growth tube, and both were placed in the reactor tube before heating. Argon with a purity of 99.996% was used as carrier gas and flew through the furnace during the entire sublimation. The flow rate was about 30mL/min [37] and it was so small that an over-night running did not significantly change the oxygen concentration in the laboratory even without a fume

المنارة للاستشارات
www.manaraa.com

hood. Heat was applied to the tube following a specific heating profile [37], as shown in Figure 5.5, to control the areas in which the materials were deposited. The heating profile was approximately measured by a thermometer (Omega HH12A) and could be adjusted by changing the relative positions of heating wire turns. The source temperature was controlled

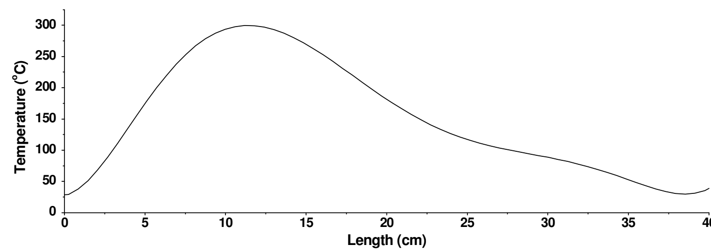

Figure 5.5 The temperature profile of the furnace.

at 300°C to avoid any residue or byproducts [37], and the variation was less than 5°C. The distillation lasted 48 hours which is much longer than that in [37]. However, after the distillation, only a small amount of pentacene was deposited in the crystal growth tube, and there was lots of black residue left in the source tube which should not happen according to [37]. More experiments are needed to optimize the distillation conditions.

5.6 Fabrication of pentacene ACT devices

Since pentacene is insoluble in most solvents, it was planned to fabricate the devices using standard liftoff photolithographic techniques. It took three steps to make a whole device. In the first step, mask 1 was used to pattern IDTs, parabolic SAW beam compressors and Schottky electrodes. Then, a 250nm-thick aluminum film was deposited on a 2-inch $LiNbO_3$ substrate to form those parts defined by mask 1. In the second step, Ohmic electrodes and bonding pads were patterned by mask 2, and a 250nm-thick gold film was then deposited to form the Ohmic electrodes and the bonding pads. In the third step, mask 3

www.manaraa.com

was used to pattern a pentacene charge transfer channel. Then the channel was form by depositing a 1μm-thick pentacene film. The pentacene film was deposited by thermal evaporation in a high vacuum chamber with base pressure 5×10^{-6}torr.

The first two steps were easily done. However, there was some trouble in the third step to make the pentacene charge transfer channel using standard liftoff technique. The trouble was the adhesion between pentacene and the $LiNbO_3$ substrate was so weak that the pentacene was easily peeled off from the substrate. After the deposition of pentacene, when isopropanol was used to remove the photoresist, the pentacene channel was ruined as well.

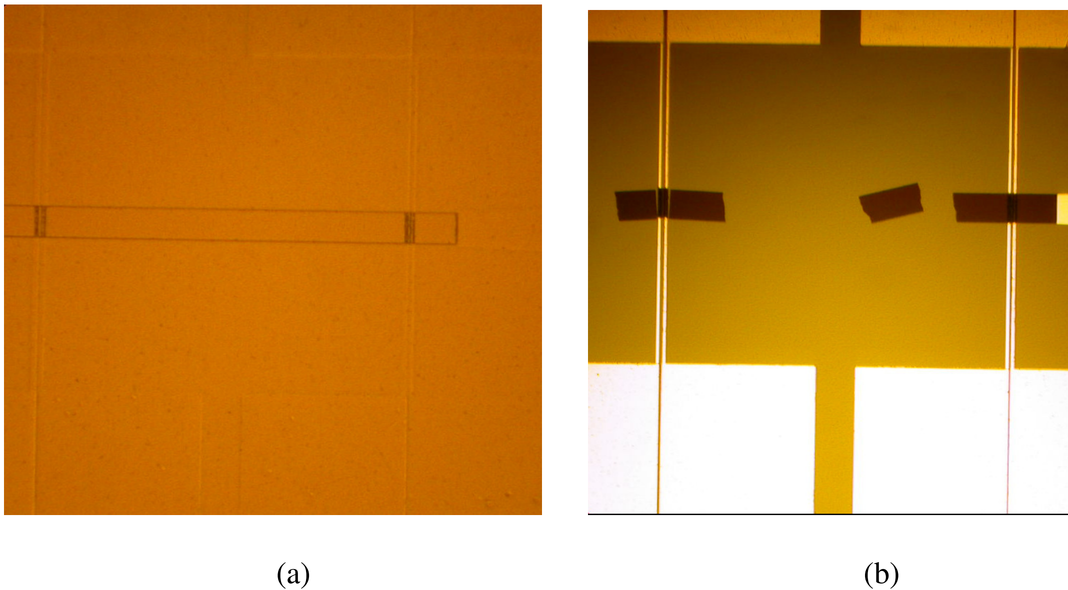

(a) (b)

Figure 5.6 Photos of the pentacene layer. (a) before removing photoresist, (b) after removing photoresist.

Figure 5.6 shows photos of the pentacene layer before and after removing the photoresist. As shown in Figure 5.6 (a), the film was homogeneous and there was no apparent pattern on it, which means the deposition of pentacene was successful. However, after removing the

المنارة للاستشارات
www.manaraa.com

photoresist, not only the unwanted pentacene but most of the pentacene needed to form the charge transfer channel was removed. The channel line was broken into many small parts, as shown in Figure 5.6 (b). Several ways were tried to reduce the damage to the pentacene channel, which include using different organic solvents, such as acetone and isopropanol, to remove the photoresist; reducing the agitation during the photoresist removal; and depositing

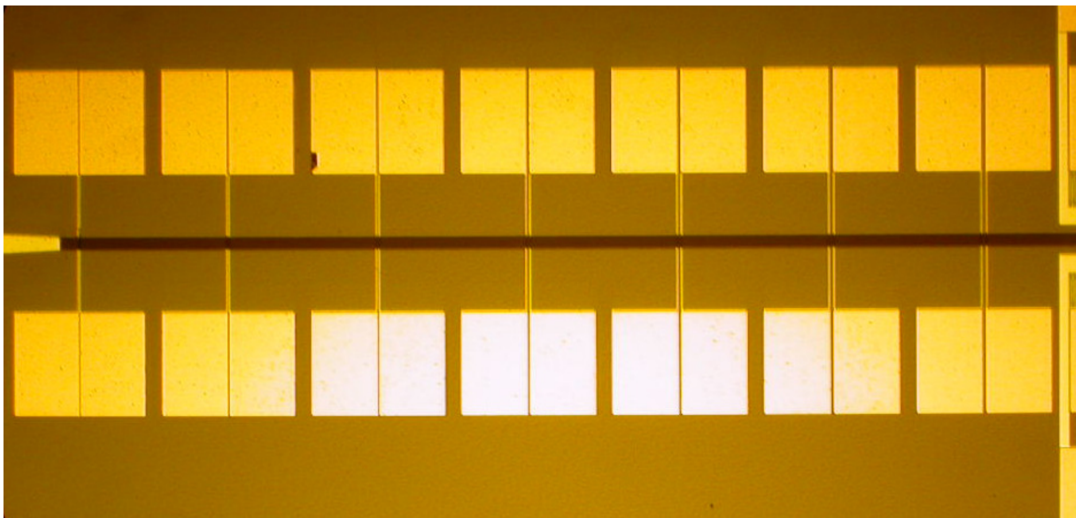

Figure 5.7 Photo of a good pentacene charge transfer channel.

pentacene films at different rates from 1Å/sec to 5Å/sec. But none of them showed the acceptable results. Sometimes, a good result could be obtained, as shown in Figure 5.7. However, the reproducibility was very poor. The reasons are still under investigation.

5.7 Conclusions

A design of pentacene ACT was proposed in this work. The minimum requirement of the electrical power was calculated for a SAW with a wavelength of 12µm. In order to reduce

المنارة للاستشارات
www.manaraa.com

the required electrical drive power, a parabolic SAW beam compressor was used and the detailed design of the parabolic compressor was given. Since commercially available pentacene contains nonnegligible amounts of impurities and will harm the performance of this novel ACT device, a temperature gradient furnace was set up to distill pentacene. The device could be fabricated using standard liftoff photolithographic techniques. However, there were some problems fabricating the pentacene charge transfer channel by liftoff techniques. Solutions are under investigation.

المنارة للاستشارات

www.manaraa.com

CHAPTER 6. CONCLUSIONS AND FUTURE WORK

6.1 Conclusions

SAW filters were fabricated on an Mg-doped GaN epilayer using standard liftoff lithographic techniques. The measurement of the time response showed that these devices had very weak output signals. The center frequencies were 136.09MHz, 114.48MHz and 98.64MHz for devices with wavelengths of 40μm, 48μm and 56μm, respectively. No change of the reflection coefficient was detectable using the available network analyzer for all devices around the center frequencies. The insertion loss for all devices was higher than 80dB which showed that K^2 for the Mg-doped GaN epilayers had an upper bound of ~0.0001%. This is extremely small, much less than other III-V materials, and so this material does not appear to be promising for SAW applications.

A design of a pentacene ACT device was discussed in this work according to a previous proposal of Woods [17]. Because the charge mobility of pentacene is very small, the minimum requirement of the SAW power per unit acoustic aperture is very high. In order to reduce the required electrical drive power, a parabolic SAW beam compressor was used and the detailed design of the parabolic compressor was given. It is known that commercially available pentacene contains nonnegligible amounts of impurities so that its charge mobility will be low. Therefore, a temperature gradient furnace was set up to distill pentacene to improve the carrier mobility. The device is expected to be fabricated using standard liftoff photolithographic techniques. However, some problems were met when the pentacene charge transfer channel was fabricated. Solutions are under investigation.

www.manaraa.com

6.2 Future work

The research of pentacene ACT device is still in the initial stage. Some important future work is:

1. Optimize the fabrication of pentacene charge transfer channel, and improve the reproducibility. The key point here is to increase the adhesion between pentacene and the $LiNbO_3$ substrate. Two ways might be considered: a) increase the substrate temperature when depositing pentacene film; b) deposit some other material which can act as an adhesive between pentacene and the substrate.
2. Purify pentacene using a temperature gradient furnace. This will increase the charge mobility in pentacene, which in turn reduces the minimum requirement of the electrical drive power.
3. Fabricate devices on a $Bi_{12}GeO_{20}$ substrate. Since the SAW velocity in a $Bi_{12}GeO_{20}$ substrate is much slower than that in a $LiNbO_3$ substrate, the required electrical power will be dramatically reduced.
4. Use SAWs with shorter wavelengths. Shorter wavelengths mean higher frequencies. Since SAW acts as a "clock" in an ACT device, SAWs with higher frequencies can sample signals with higher frequencies. Using shorter wavelength SAWs can reduce the power requirement as well.
5. Use other materials as the charge transfer channel, such as nanocrystalline silicon and ZnO. These materials have much higher carrier mobility. The power required becomes so small that a SAW beam compressor is unnecessary. This will greatly simplify the design of the ACT devices. These materials can be easily deposited as well.

المنارة للاستشارات
www.manaraa.com

APPENDIX A. EQUATIONS OF MOTION IN A HOMOGENEOUS SOLID MEDIUM [14]

Consider an infinitesimal volume element within a homogeneous solid medium with sides of length $\Delta x_1, \Delta x_2, \Delta x_3$, parallel to the x_1, x_2, x_3 axes, as shown in Figure 2.1, the stress exerted on each face of the infinitesimal volume element can be divided into three

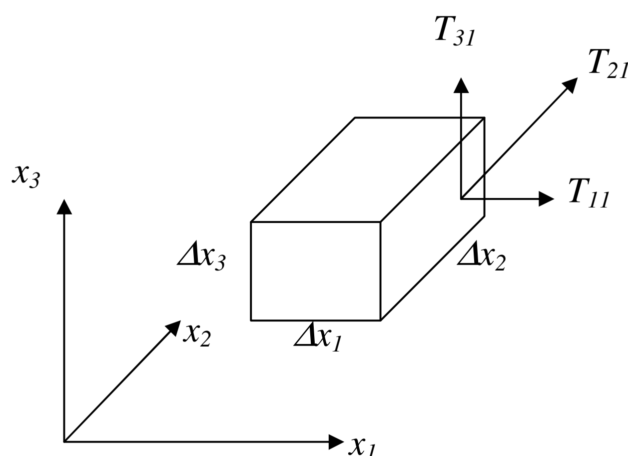

Figure 2.1 Forces exerted on an infinitesimal volume element.

components along the three axes. Assume the x_1 component of the stress acting on plane $x_1=0$ is T_{11}, since Δx_1 is small, the x_1 component of the stress acting on plane $x_1=\Delta x_1$ will be $T_{11}+\frac{\partial T_{11}}{\partial x_1}\Delta x_1$. Similarly, the x_1 components of the stresses acting on planes $x_2=0$ and $x_2=\Delta x_2$ are T_{12} and $T_{12}+\frac{\partial T_{12}}{\partial x_2}\Delta x_2$; the x_1 components of the stresses acting on planes $x_3=0$ and

www.manaraa.com

$x_3=\Delta x_3$ are T_{13} and $T_{13}+\frac{\partial T_{13}}{\partial x_3}\Delta x_3$. Therefore, along x_1 axis, the total force exerted on the infinitesimal volume element is

$$\left(T_{11}+\frac{\partial T_{11}}{\partial x_1}\Delta x_1-T_{11}\right)\Delta x_2\Delta x_3+\left(T_{12}+\frac{\partial T_{12}}{\partial x_2}\Delta x_2-T_{12}\right)\Delta x_1\Delta x_3+\left(T_{13}+\frac{\partial T_{13}}{\partial x_3}\Delta x_3-T_{13}\right)\Delta x_1\Delta x_2$$
$$=\left(\frac{\partial T_{11}}{\partial x_1}+\frac{\partial T_{12}}{\partial x_2}+\frac{\partial T_{13}}{\partial x_3}\right)\Delta x_1\Delta x_2\Delta x_3$$

If there are no body forces exerted, by Newton's second law, the equation of motion of the infinitesimal volume element along the x_1 direction is

$$\rho\Delta x_1\Delta x_2\Delta x_3\frac{\partial^2 u_1}{\partial t^2}=\left(\frac{\partial T_{11}}{\partial x_1}+\frac{\partial T_{12}}{\partial x_2}+\frac{\partial T_{13}}{\partial x_3}\right)\Delta x_1\Delta x_2\Delta x_3, \qquad \text{(A.1)}$$

where ρ is the density of the medium, u_1 is the x_1 component of the displacement of the infinitesimal volume element. Eliminating $\Delta x_1\Delta x_2\Delta x_3$ reduces (A.1) to

$$\rho\frac{\partial^2 u_1}{\partial t^2}=\frac{\partial T_{11}}{\partial x_1}+\frac{\partial T_{12}}{\partial x_2}+\frac{\partial T_{13}}{\partial x_3}. \qquad \text{(A.2a)}$$

Similarly, the equations of motion of the infinitesimal volume element along the x_2 and x_3 directions are

$$\rho\frac{\partial^2 u_2}{\partial t^2}=\frac{\partial T_{21}}{\partial x_1}+\frac{\partial T_{22}}{\partial x_2}+\frac{\partial T_{23}}{\partial x_3}, \qquad \text{(A.2b)}$$

$$\rho\frac{\partial^2 u_3}{\partial t^2}=\frac{\partial T_{31}}{\partial x_1}+\frac{\partial T_{32}}{\partial x_2}+\frac{\partial T_{33}}{\partial x_3}, \qquad \text{(A.2c)}$$

where u_2 and u_3 are the x_2 and x_3 components of the displacement of the infinitesimal volume element, respectively. (A.2a), (A.2b) and (A.2c) are the equations of motion of each

المنارة للاستشارات
www.manaraa.com

infinitesimal volume element of the elastic medium in Cartesian coordinate system. They can be written as

$$\rho \frac{\partial^2 u_i}{\partial t^2} = \sum_{j=1}^{3} \frac{\partial T_{ij}}{\partial x_j} \qquad (i=1,\ 2,\ 3). \tag{A.3}$$

Using the Einstein summation convention which implies that when an index occurs more than once in the same expression, the expression is implicitly summed over all possible values for that index, equation (A.3) can be reduced to

$$\rho \frac{\partial^2 u_i}{\partial t^2} = \frac{\partial T_{ij}}{\partial x_j} \qquad (i,\ j=1,\ 2,\ 3). \tag{A.4}$$

المنارة للاستشارات

www.manaraa.com

APPENDIX B. WAVE EQUATIONS IN A PIEZOELECTRIC ELASTIC MEDIUM [14]

In a piezoelectric material, a strain will cause an electric field. That electric field in turn will affect the strain. Therefore, the stress depends on not only the strain but also the electric field, and it can be expressed as

$$T_{ij} = c^E_{ijkl} S_{kl} - e_{kij} E_k, \quad (i, j, k, l = 1, 2, 3) \tag{B.1}$$

where c^E_{ijkl} is the elastic constant when the electric field is a constant, e_{kij} is the piezoelectric constant, and E_k is the electric field generated by the strain.

Since the wavelength of the electromagnetic wave generated by a SAW is much longer than the size of the general SAW device, the electric field can be consider static and it can be written as

$$E_k = -\frac{\partial \Phi}{\partial x_k} \qquad (k = 1, 2, 3). \tag{B.2}$$

Substituting (B.2) into (B.1) leads to

$$T_{ij} = c^E_{ijkl} \frac{\partial u_k}{\partial x_l} + e_{kij} \frac{\partial \Phi}{\partial x_k}. \tag{B.3}$$

Substitution of (B.3) into (A.4) yields

$$\rho \frac{\partial^2 u_i}{\partial t^2} = c^E_{ijkl} \frac{\partial^2 u_k}{\partial x_l \partial x_k} + e_{kij} \frac{\partial^2 \Phi}{\partial x_k \partial x_j}. \tag{B.4}$$

Furthermore, for an insulator, the electric displacement must obey the Poisson equation

المنارة للاستشارات
www.manaraa.com

$$\frac{\partial D_j}{\partial x_j} = 0. \tag{B.5}$$

In a piezoelectric material, the electric displacement is equal to

$$D_j = e_{jkl} S_{kl} + \varepsilon_{jk} E_k, \tag{B.6}$$

where ε_{jk} is the components of the dielectric constant of the piezoelectric material. Substituting (B.6) into (B.5) gives

$$e_{jkl} \frac{\partial^2 u_k}{\partial x_l \partial x_j} - \varepsilon_{jk} \frac{\partial^2 \Phi}{\partial x_k \partial x_j} = 0. \tag{B.7}$$

Hence, the wave equations in a piezoelectric material are described by the equation set of (B.4) and (B.7).

المنارة للاستشارات
www.manaraa.com

REFERENCES

[1] Lord Rayleigh, "On waves propagating along the plane surface of an elastic solid", Proc. London Math. Soc., vol. 7, pp. 4-11, Nov. 1885.

[2] R. M. White and F. W. Voltmer, "Direct piezoelectric coupling to surface elastic waves", Appl. Phys. Lett., vol. 17, pp. 314-316, 1965.

[3] C. C.W. Ruppel, R. Dill, A. Fischerauer, G. Fischerauer, W. Gawlik, J. Machui, F. Müller, L. Reindl, W. Ruile, G. Scholl, I. Schropp, and K. Ch. Wagner, “SAW Devices for Consumer Communication Applications”, IEEE Trans. Ultrason. Ferroelect. Freq. Contr., 40, 438-452, 1993.

[4] C. S. Hartmann, "System impact of modern Rayleigh wave technology", Rayleigh-Wave Theory and Application, E. A. Ash and E. G. S. Paige, Eds. New York: Springer-Verlag, pp. 236-253, 1985.

[5] C. Campbell, “Surface Acoustic Wave Devices and Their Signal Processing Applications”, ACADEMIC PRESS, 1989.

[6] W. R. Smith, “Basics of the SAW interdigital transducer”, in J. H. Collins and L. Masotti (eds). Computer-Aided Design of Surface-Acoustic Wave Devices, Elsevier, New York, pp. 25-63, 1976.

[7] M. J. Hoskins, H. Morkoc, and B. J. Hunsinger, “Charge transport by surface acoustic waves in GaAs”, Appl. Phys. Lett. 41, 332-334, 1982.

[8] M. J. Hoskins and B. J. Hunsinger, “Recent Developments in acoustic charge transport devices”, IEEE Ultrasonics Symp., pp. 439-450, 1986.

المنارة للاستشارات
www.manaraa.com

[9] B. J. Hunsinger, "SAWs enable the advent of the signal microprocessor development station", Proc. IEEE Ultrasonics Swnp., pp. 225-229, 1990.

[10] J. E. Bales, M. J. Hoskins, and P, H. Sahm, "A GaAs ACTiIC programmable wide-hand analog signal processor", Proc. 1990 IEEE GaAs IC Symp., pp. 23-26, 1990.

[11] R. W. Miller and R. J. Kansy, "Acoustic charge transport digitally programmable transversal filter development", 1990 IEEE MTT-S Symp. Proc., pp. 1111-1114, 1990.

[12] A. J. Vigil, A. W. Hull, L. P. Solie, M. J. Miller, R. J. Kansy, and D. A. Fleisch, “Applications of Acoustic Charge Transport”, IEEE Trans. Ultrason. Ferroelect. Freq. Contr., 40, 488-495, 1993.

[13] R. L. Miller, C. E. Nothnick, and D. S. Bailey, “Acoustic Charge Transport: Device Technology and Applications”, Artech House, 1992.

[14] Y. L. Wu, “Surface Acoustic Wave Theory and Its Applications in Electronic Technology”, National Defense Industry Press, 1983.

[15] E. Dieulesaint and D. Royer, “Elastic Waves in Solids”, John Wiley & sons, 1974.

[16] A. A. Oliner, “Acoustic Surface Waves”, Topics in Applied Physics, Springer-Verlag Berlin Heidelberg, 1978.

[17] R. C. Woods, “Charge transfer device using organic semiconductor”, unpublished, 2004.

[18] B. A. Auld, “Acoustic fields and waves in solids”, Vol. II. 2nd ed. Malabar: R.E. Krieger, 1990.

[19] W. J. Tanski, S. W. Merritt, R. N. Sacks, D. E. Cullen, E. J. Branciforte, R. D. Carroll, and T. C. Eschrich, “Heterojunction acoustic charge transport devices on GaAs”, Appl. Phys. Lett., 52, pp. 18-20, 1988.

المنارة للاستشارات

www.manaraa.com

[20] R. K. Hayden, R. C. Woods, S. Kumagai, K. Yamanouchi, and R, Grey "Comparison of quantum well and single heterojunction structures for acoustic charge transfer devices", J. Appl. Phys., 79, pp. 8792-8797, 1996.

[21] S. H. Lee, H. H. Jeong, S. B. Bae, H. C. Choi, J. H. Lee, and Y.H. Lee, "Epitaxially grown GaN thin-film SAW filter with high velocity and low insertion loss", IEEE Trans. Electron. Devices, 48, pp. 524-529, 2001.

[22] R. C. Woods, and F. A. Boroumand, "Comments on 'Epitaxially Grown GaN Thin-Film SAW Filter with High Velocity and Low Insertion Loss'", IEEE Trans. Electron. Devices, 53, pp. 173-176, 2006.

[23] G. D. O'Clock Jr., and M. T. Duffy, "Acoustic surface wave properties of epitaxially grown aluminum nitride and gallium nitride on sapphire", Appl. Phys. Lett., 23, pp. 55-56, 1973.

[24] S. C. Jain, M. Willander, J. Narayan, and R. Van Overstraeten, "III–nitrides: Growth, characterization, and properties", J. Appl. Phys., 87, pp. 965-1006, 2000.

[25] J. K. Kim, J. L. Lee, J. W. Lee, H. E. Shin, Y. J. Park, and T. Kim, "Low resistance Pd/Au ohmic contacts to *p*-type GaN using surface treatment", Appl. Phys. Lett., 73, pp. 2953-2955, 1998.

[26] C. S. Hartmann, D.T. Bell, and R. Rosenfeld, "Impulse model design of acoustic surface-wave filters", IEEE Trans. Microwave Theory and Techniques, MTT-21, pp. 162-175, 1973.

[27] V. Y. Butko, X. Chi, D. V. Lang, and A. P. Ramirez, "Field-effect transistor on pentacene single crystal", Appl. Phys. Lett., 83, pp. 4773-4775, 2003.

المنارة للاستشارات

www.manaraa.com

[28] M. K. Roy, “A Rayleigh Wave Beam Compressor Using Δv/v-Type Guidance”, IEEE Trans. On Sonics and Ultrasonics, Su-23, pp 276-279, 1976.

[29] R. A. Becker, and D. H. Hurlburt, “Wideband LiNbO3 elastic convolver with parabolic horns”, Proc.1979 IEEE Ultrasonics Symp., pp. 729-731, 1979.

[30] P. Defranould, and C. Maerfeld, “Acoustic convolver using multistrip beamwidth compressors”, Proc. 1974 IEEE Ultrasonics Symp., pp. 224-227, 1974.

[31] H. P. Grassl, and H. Engan, “Small-aperture focusing chirp transducers vs. diffraction-compensated beam compressors in elastic SAW convolvers”, IEEE Trans. Sonics & Ultrasonics, SU-32, pp. 675-684, 1985.

[32] B. J. Darby, D. Gunton, and M. F. Lewis, “The design and performance of a small efficient SAW convolver”, Proc. 1980 IEEE Ultrasonics Symp., pp. 53-58, 1980.

[33] R. C. Weast, “Handbook of chemistry and physics”, 58th. Ed., CRC (Cleveland), pp. C-793, E-81, E-82, F-85, F-321, 1977.

[34] R. B. Campbell, J. M. Robertson, and J. Trotter, “The crystal and molecular structure of pentacene”, Acta Cryst., 14, pp. 705-711, 1961.

[35] D. C. Malocha, “Elastic convolver with a modified multistrip coupler compressor”, Proc. 1981 IEEE Ultrasonics Symp., pp. 192-195, 1981.

[36] O. D. Jurchescu, J. Baas, and T. T. M. Palstra, “Effect of impurities on the mobility of single crystal pentacene”, Appl. Phys. Lett., 84, pp. 3601-3603, 2004.

[37] L. B. Roberson, J. Kowalik, L. M. Tolbert, C. Kloc, R. Zeis, X. Chi, R. Fleming, and C. Wilkins, “Pentacene Disproportionation during Sublimation for Field-Effect Transistors”, J. Am. Chem. Soc., 127, pp. 3070-3075, 2005.

المنارة للاستشارات

www.manaraa.com

[38] Rama Corporation, “Engineering Guide”,

http://www.ramacorporation.com/engineer/Engineerweb.pdf, 06/06/2006

المنارة للاستشارات

www.manaraa.com

ACKNOWLEDGEMENTS

I would like to thank Dr. Clive Woods for giving me an opportunity to work on this project. I would also like to thank Dr. Jiming Song and Dr. Kai-Ming Ho for serving on my committee. I want to thank Dr. Gary Tuttle at the Microelectronics Research Center for giving me lots of useful advice and allowing me to use the equipments. I also want to thank all other people who helped me with various aspects of conducting research and the writing of this thesis.

للاستشارات المنارة

www.manaraa.com